

Open clusters in Auriga OB2*

Amparo Marco^{1,2,†} and Ignacio Negueruela¹

¹*DFISTS, EPS, Universidad de Alicante, Carretera San Vicente del Raspeig s/n, E03690, San Vicente del Raspeig, Spain*

²*Department of Astronomy, University of Florida, 211 Bryant Space Science Center, Gainesville, FL 32611, USA*

Accepted 2016 March 14. Received 2016 March 11; in original form 2016 January 7

ABSTRACT

We study the area around the H II region Sh 2-234, including the young open cluster Stock 8, to investigate the extent and definition of the association Aur OB2 and the possible role of triggering in massive cluster formation. We obtained Strömgren and J, H, K_s photometry for Stock 8 and Strömgren photometry for two other cluster candidates in the area, which we confirm as young open clusters and name Alicante 11 and Alicante 12. We took spectroscopy of ~ 33 early-type stars in the area, including the brightest cluster members. We calculate a common distance of $2.80^{+0.27}_{-0.24}$ kpc for the three open clusters and surrounding association. We derive an age 4–6 Ma for Stock 8, and do not find a significantly different age for the other clusters or the association. The star LSV +34°23, with spectral type O8 II(f), is likely the main source of ionization of Sh 2-234. We observe an important population of pre-main sequence stars, some of them with disks, associated with the B-type members lying on the main-sequence. We interpret the region as an area of recent star formation with some residual and very localized ongoing star formation. We do not find evidence for sequential star formation on a large scale. The classical definition of Aur OB2 has to be reconsidered, because its two main open clusters, Stock 8 and NGC 1893, are not at the same distance. Stock 8 is probably located in the Perseus arm, but other nearby H II regions whose distances also place them in this arm show quite different distances and radial velocities and, therefore, are not connected.

Key words: techniques: photometric – techniques: spectroscopic – stars: early-type – stars: evolution – Hertzsprung–Russell and colour–magnitude diagrams – open clusters and associations: individual: Alicante 11 – open clusters and associations: individual: Alicante 12

1 INTRODUCTION

Stellar associations are large and loose, comoving stellar groups of low-density stars often associated with smaller open cluster groups. OB associations contain O and/or early B-type stars. They must be young (≤ 30 Ma) because they are unstable against Galactic tidal forces. Therefore, most of their low-mass members are still found in the pre-main sequence (PMS) phase. They are excellent targets for detailed studies of the initial mass function and the star formation history because they represent a place where the star formation process has been completed recently. Their space distribution also provides useful information about the spiral

structure of the Galaxy (Blaauw 1964; Preibisch & Zinnecker 2007).

OB associations are the natural outcome of star-formation processes in giant molecular clouds (GMCs) in most Milky Way environments. These large clouds demonstrate hierarchical structure in both time and space, resulting in the formation of star clusters that are not bound gravitationally to one another, but share a common distance. A well-studied example of such processes is the W3 region, which contains several small embedded clusters surrounding the optically visible cluster IC 1795 (Bik et al. 2012; Román-Zúñiga et al. 2015; Kiminki et al. 2015). A more dispersed population of early-type stars seems to connect it with IC 1805, the ionizing cluster of W4, which includes a few early O-type stars. The nearby cluster IC 1848, ionizing W5, is also likely connected. Overall stars traditionally considered to belong to Cas OB6 cover more than 6 degrees on the sky. Other examples of large star-forming regions containing moderately massive clusters include the G305 re-

* Partially based on observations collected at the Jacobus Kapteyn Telescope, the Telescopio Nazionale Galileo and the Nordic Optical Telescope (La Palma) and at the 1.50-m telescope at Observatoire de Haute Provence (CNRS), France.

† E-mail: amparo.marco@ua.es (AM)

gion, centred on the Danks 1 and 2 clusters (Hindson et al. 2013, and references therein) and the Carina Nebula (e.g. Preibisch et al. 2011). Other GMCs, such as W33 (Messineo et al. 2015) or W51, lack the central massive clusters, and will very likely evolve into dispersed associations, similar to Cyg OB2 (Wright et al. 2014).

The Perseus arm has been proposed as one of the two main spiral arms of the Galaxy (Churchwell et al. 2009). It emerges from behind obscuring clouds in the Local arm around $l = 75^\circ$ and over a significant fraction of the northern sky, it is clearly delineated by early-type luminous stars (as first realised by Morgan et al. 1953). Between $l = 100^\circ$ and 140° , the Perseus arm contains both large active star-forming regions, and more evolved associations, with ages between ~ 10 and ~ 20 Ma. Among them, some are dispersed and contain small clusters (Cas OB2/OB4/OB5/OB7), while other have massive central clusters, such as the twin clusters NGC 869/884 at the core of Per OB1 or NGC 663 and NGC 654, defining Cas OB8. However, beyond $l = 140^\circ$ stellar and molecular tracers of the Perseus arm suddenly become very rare. Cloud complexes identified with the Perseus arm are seen again in the third galactic quadrant (already at $l \approx 215^\circ$), but its stellar tracers are still scarce (Vázquez et al. 2008). Partly because of this absence of tracers, we still lack a complete picture of the extent of the Perseus Arm towards the Third Quadrant, and the connection between the Local Feature and the major spiral design (Vázquez et al. 2008; see a recent discussion in Foster & Brunt 2015). Recently, Choi et al. (2014) have used trigonometric parallaxes for water masers in massive star-forming regions to trace the Perseus Arm in the second and third quadrants. They find a number of tracers of the Perseus arm around $l = 190^\circ$, with distances clustered around 2 kpc, but again no tracers are found between $l = 140^\circ$ and $l = 180^\circ$. Over this longitude range, there are a number of young open clusters with distances around ~ 4 kpc at $l = 150^\circ$ and ~ 5 kpc at $l \sim 180^\circ$ (Negueruela & Marco 2003, and references therein). They seem to delineate a poorly-populated spiral arm, but their distance is closer than expected for the position of the continuation of the Cygnus (+II) arm in models such as those of Vallée (2015).

To help casting light on these issues, the aim of this work is to clarify the extent and definition of what has traditionally known as association Aur OB2. Aur OB2 was identified as a distant and compact association lying behind Aur OB1, with boundaries $l = 172^\circ$ - 174° and $b = -1.8^\circ$ to $b = +2.0^\circ$ (Humphreys 1978). The star-forming open cluster NGC 1893, containing five O-type stars, was considered the core of this association, but most modern studies based on accurate photometry (Marco et al. 2001; Fitzsimmons 1993) and spectroscopy (Negueruela et al. 2007) agree on a distance around 5 kpc for NGC 1893, incompatible with the distance determined to other presumed members (Humphreys 1978). Visually, IC 410, the H II region illuminated by NGC 1893, seems to form part of a single complex of illuminated clouds together with IC 417 and IC 405. This is just an illusion, as IC 405 is a completely unrelated nebula, associated to a foreground ($d \approx 450$ pc) cloud illuminated by the runaway star AE Aur, believed to have been ejected from the Orion Cloud (France et al. 2004, and references therein). IC 417, also known as Sh2-234, is the H II region illuminated by the open cluster Stock 8. Its Galactic coordi-

nates are $l = 173^\circ.37$ and $b = -0^\circ.18$. In this paper, we present a photometric and spectroscopic study of Stock 8, the diffuse population of OB stars generally assigned to Aur OB2, and two other young open clusters that we identify in its vicinity.

There have been a few previous studies of Stock 8 and surroundings. However, the extent of the cluster itself has not been clearly defined. The name Stock 8 has been traditionally given to a strong stellar concentration that seems to be embedded in the nebula associated with Sh 2-234. Mayer & Macak (1971) carried out an spectroscopic and *UBV* photoelectric photometry study of 11 bright stars in its surroundings, finding a common distance for Stock 8 and some of the OB stars in its vicinity (a few arcminutes to the west; see Fig. 1), namely, a distance modulus (DM) of 12.36 magnitudes (2965 pc). Malysheva (1990) used *UBV* photographic photometry of ~ 66 stars brighter than $V = 16$ inside an angular diameter of $20'$ from Stock 8, and obtained a DM of 11.39 magnitudes (~ 1897 pc) and an age of ~ 12 Ma. Jose et al. (2008) took *UBVI_c* CCD photometry of the compact cluster and found a cluster radius of $\sim 6'$, a variable reddening within the cluster region, going from $E(B - V) = 0.40$ to 0.60 mag, and a distance of 2.05 ± 0.10 kpc. They detected a significant number of young stellar objects (YSOs) inside the cluster and in a Nebulous Stream towards the east side of the cluster (see Fig. 1). The YSOs lying in the Nebulous Stream were found to be younger than the stars in Stock 8. They conclude that the morphology of the region seems to indicate that the ionization/shock front caused by the ionizing sources located inside and west of Stock 8 has not reached the Nebulous Stream and the star formation activity in both regions may be independent.

In this paper, we study a much larger area of $\sim 40' \times 40'$, where we find Stock 8 and two candidates to young clusters, as well as a large number of early-type stars spread over the whole area. We aim to determine accurately the distance to all these objects and analyze how the stellar formation process has developed. The paper is organized as follows. In Section 2 we present the photometric and spectroscopic data used to make the subsequent analysis. This analysis, including the determination of spectral types for individual stars, and the reddening, distance and age for the three clusters studied, is developed in Section 3. In Section 4 we comment the impact of our results on the history of star formation and the position in the Milky Way of Stock 8 and surroundings. Finally, we enumerate our conclusions.

2 OBSERVATIONS AND DATA

2.1 Optical photometry

We obtained Strömgren photometry of three fields in the area of study with the 1-m Jacobus Kapteyn Telescope (JKT) at the Roque de los Muchachos Observatory (La Palma, Spain) during a run in 2003 February, 9–16. The telescope was equipped with the 2048×2048 SITe1 chip CCD and the four Strömgren *uvby* and the narrow and wide *H β* filters. The camera covers a field of $10' \times 10'$ and has a pixel scale of $0''.33 \text{ pixel}^{-1}$.

The first field was the area traditionally assigned to Stock 8, which was observed on the nights of 2003 February,

Table 1. Clusters observed from the JKT in February 2003. The top panel contains the target fields, while the bottom panel includes the clusters that contain the photometric standards. The coordinates are those provided by the WEBDA database: <http://www.univie.ac.at/webda/> (Netopil et al. 2012), except for the two newly defined clusters.

Name	RA(J2000)	Dec(J2000)
Stock 8	05h 28m 08.0s	+34° 25' 42"0
Alicante 11	05h 27m 36.2s	+34° 45' 19"0
Alicante 12	05h 28m 20.3s	+34° 47' 13"5
NGC 2244	06h 31m 55.0s	+04° 56' 30"0
NGC 2169	06h 08m 24.0s	+13° 57' 54"0
NGC 1502	04h 07m 40.4s	+62° 20' 59"1
NGC 1039	20h 23m 10.6s	+40° 46' 22"4
NGC 869	02h 19m 04.4s	+57° 08' 07"8
NGC 884	02h 22m 00.6s	+57° 08' 42"1

9–10. For each frame, we obtained 7 series of different exposure times in each filter to achieve accurate photometry for a broad magnitude range. The central position for the cluster and the exposure times used are presented in Table 1 and Table 2, respectively

The other two fields observed were centred on two stellar aggregates that we considered open cluster candidates. Subsequently to our observations, these open clusters have appeared in the literature as cluster candidates with the names of FSR 777 (Froeblich et al. 2007) and Kronberger 1 (Kronberger et al. 2006). These two objects are confirmed as young open clusters here and named Alicante 11 and Alicante 12, respectively. The frames, taken on the nights of 2003 February, 15–16, were centred on the coordinates displayed in Table 1. We obtained 7 series of different exposure times for Alicante 11 and 3 series for Alicante 12. The exposure times used are presented in Table 2. Since Stock 8 is partially embedded in dark nebulosity, exposure times for this field were longer than those in the other two fields. Our intention was to reach an absolute magnitude that would allow us to trace the whole sequence of B types. As will be seen later, this was effectively achieved.

Standard stars were observed throughout the run in the clusters NGC 869, NGC 884, NGC 1039, NGC 1502, NGC 2169 and NGC 2244, using the exposure times suitable to obtain good photometric values for all stars selected as standards in these clusters. The central positions for the clusters and the exposure times used are presented in Table 1 and Table 2, respectively. If any of the selected standards turned out to be saturated, we repeated the observations with a shorter exposure time.

We reduced the frames for all clusters with IRAF¹ routines for the bias and flat-field corrections. Photometry was obtained by point-spread function (PSF) fitting using the DAOPHOT package (Stetson 1987) provided by IRAF. The apertures used are of the order of the full width at half max-

Table 2. Log of the optical photometric observations taken at the JKT in February 2003.

Filter	Exposure times(s)	
	Long times	Short times
Stock 8		
<i>u</i>	1800	400
<i>v</i>	500	175
<i>b</i>	200	100
<i>y</i>	150	50
$H\beta_n$	1800	400
$H\beta_w$	200	100
Alicante 11		
<i>u</i>	450	100
<i>v</i>	180	40
<i>b</i>	100	20
<i>y</i>	50	8
$H\beta_n$	400	100
$H\beta_w$	60	15
Alicante 12		
<i>u</i>	450	–
<i>v</i>	180	–
<i>b</i>	100	–
<i>y</i>	50	–
$H\beta_n$	400	–
$H\beta_w$	60	–
NGC 2244		
<i>u</i>	35	20
<i>v</i>	30	20
<i>b</i>	15	10
<i>y</i>	20	5
$H\beta_n$	25	–
$H\beta_w$	10	–
NGC 2169		
<i>u</i>	50	–
<i>v</i>	30	–
<i>b</i>	20	–
<i>y</i>	20	10
$H\beta_n$	50	–
$H\beta_w$	25	–
NGC 1502		
<i>u</i>	400	–
<i>v</i>	200	–
<i>b</i>	150	–
<i>y</i>	30	10
$H\beta_n$	350	–
$H\beta_w$	30	–
NGC 1039		
<i>u</i>	50	–
<i>v</i>	30	–
<i>b</i>	20	–
<i>y</i>	20	5
$H\beta_n$	50	–
$H\beta_w$	25	5
NGC 869 and NGC 884		
<i>u</i>	600	–
<i>v</i>	350	–
<i>b</i>	200	–
<i>y</i>	100	–
$H\beta_n$	600	–
$H\beta_w$	120	–

¹ IRAF is distributed by the National Optical Astronomy Observatories, which are operated by the Association of Universities for Research in Astronomy, Inc., under cooperative agreement with the National Science Foundation

imum. In this case, we used a value of 6 pixels for each image in all filters. In order to construct the PSF empirically, we automatically selected bright stars (typically 25 stars). After this, we reviewed the candidates and we discarded those that did not reach the best conditions for a good PSF star. Once we had the list of PSF stars (≈ 20), we determined an initial PSF by fitting the best function between the 5 options offered by the PSF routine inside DAOPHOT. We allowed the PSF to be variable (of order 2) across the frame to take into account the systematic pattern of PSF variability with position on the chip.

We needed to perform an aperture correction of 26, 25 and 30 pixels for the u , v and b filters, respectively. The aperture correction for the rest of the filters: y , $H\beta_n$ and $H\beta_w$ was of 28 pixels. The atmospheric extinction corrections were performed using the RANBO2 program, which implements the method described by Manfroid (1993). Finally, we obtained the instrumental magnitudes for all stars.

The selection of standard stars has been explained in Marco & Negueruela (2013). In this work, we used two new open clusters that fulfilled the requirements to provide standard stars. The list of newly adopted standard stars and their photometric data to be used in the transformations of CCD Strömberg photometry of open clusters are given in Table 3.

With the standard stars, we transformed the instrumental magnitudes to the standard system using the PHOTCAL package inside IRAF. We implemented the following $uvby$ transformation equations, after Crawford & Barnes (1970a) and the β transformation equation after Crawford & Mander (1966):

$$V = (-4.937 + A) - 0.110(b - y) + y_i \quad (1)$$

$$\pm 0.009 \pm 0.035$$

$$(b - y) = (0.231 + B) + 1.037(b - y)_i \quad (2)$$

$$\pm 0.002 \pm 0.013$$

$$m_1 = (-0.668 + C) + 0.923m_{1i} - 0.159(b - y) \quad (3)$$

$$\pm 0.047 \pm 0.051 \pm 0.031$$

$$c_1 = (0.016 + D) + 1.020c_{1i} - 0.202(b - y) \quad (4)$$

$$\pm 0.011 \pm 0.011 \pm 0.030$$

$$\beta = (1.198 + E) + 0.703\beta_i \quad (5)$$

$$R^2 = 0.97$$

where each coefficient is given with the error resulting from the transformation. The values of A, B, C, D and E represent zero points whose values are different for each night. These values are provided in Table 4.

The number of stars that can be detected in all filters is limited by the long exposure time in the u filter. We selected for the analysis all stars with good photometry (photometric errors ≤ 0.05 mag) in all six filters. We identify these stars on the images in Figures 2, 3 and 4 for each field observed.

We have obtained $uvby\beta$ CCD photometry for 163 stars in the cluster Stock 8, reaching a magnitude limit $V \approx 16$. In Table 10, we list their coordinates in J2000. The second column cross-references with the near-infrared (near-IR) photometry, indicating their number in Table 11, for those stars that have values in our near-IR photometry. For stars with

no measurements in Table 11, the last columns show JHK_s photometry from the 2MASS catalog (Skrutskie et al. 2006). The $uvby\beta$ CCD photometry is given in Table 12, where N is the number of measurements for each magnitude, colour or index and σ is the error assigned to each value. The error assigned is the standard deviation for stars with more than one measurement and the photometric errors from DAOPHOT for stars with only one measurement, with the errors in the colour and indices calculated through error propagation. In Fig. 2 we indicate with yellow open circles stars with optical photometry. The open blue squares are stars that we could detect in our near-IR photometry. Solid red squares are stars for which we obtained spectra. In Table 13 and Table 15 we list the number and the coordinates in J2000 for stars in the Alicante 11 and the Alicante 12 fields with optical photometry. In these tables we show their JHK_s photometry from the 2MASS catalog (Skrutskie et al. 2006) too. In Table 14 and Table 16 we present the resulting values for V , $b - y$, m_1 , c_1 and β for stars in Alicante 11 and Alicante 12, together with the number of measurements for each magnitude, colour or index and the error assigned for each value. These errors are calculated as above. The designation of each star is given by the number indicated on the images (Fig. 3 and Fig. 4). We obtained optical photometry for 57 stars in Alicante 11 and for 52 stars in Alicante 12.

2.2 Near-IR photometry

Near-IR JHK images were obtained in the area of the open cluster Stock 8 using NICS (Near Infrared Camera Spectrometer) on the Telescopio Nazionale Galileo (TNG) in the La Palma observatory on 14 May 2011. NICS was equipped with a HgCdTe Hawaii 1024 \times 1024 array, providing a pixel scale of $0''.25$ pixel and a field of view of $4'.2 \times 4'.2$ in its large field (LF) mode. The observations were carried out under photometric conditions.

These near-IR observations consisted of series of several integrations repeated at dithered positions on the detector. The total effective exposure, resulting from the co-addition of the jittered exposures, is 60 s for long exposures and 15 s for short exposures in all filters.

The standard reduction of near-IR data includes the dark subtraction and flat-field correction of individual frames that are median-combined to build a sky image. The sky image is subsequently subtracted from the individual frames that are then shifted and finally stacked into one single image. The procedure for obtaining the photometry from the reduced frames was the same as described in Section 2.1 for the optical images.

The next step is to transform these instrumental magnitudes to the 2MASS magnitude system (Skrutskie et al. 2006). For this, we selected those stars in our field having JHK_s magnitudes in the 2MASS catalogue with photometric errors smaller than 0.03 magnitudes in every filter (about 80 stars). A linear transformation was carried out between instrumental and 2MASS magnitudes. No colour term was needed, since a simple shift in zero point results in a good transformation. This was checked by plotting the transformed magnitudes against 2MASS magnitudes for all the stars with 2MASS magnitudes in the field, finding that the best fit corresponds to a straight line of slope 1 in all three filters.

Table 3. New adopted standard stars with their cataloged values and spectral types taken from the literature

Star	V	$b-y$	m_1	c_1	β	Spectral Type
NGC 2244						
114	7.590	0.207	-0.048	-0.081	2.608	O8.5 V
NGC 2169						
11	10.600	0.084	0.065	0.541	2.698	B8 V
15	11.080	0.130	0.109	0.944	2.864	B9.5 V
18	11.800	0.115	0.105	0.912	2.872	B9.5 V

The data are taken from Crawford (1975) and Johnson & Morgan (1953) for NGC 2244 and Perry et al. (1978) for NGC 2169. Spectral types are taken from Walborn (1971) for NGC 2244, and Perry et al. (1978) for NGC 2169.

Table 4. Values of the constants A, B, C, D and E for each night.

Night	A	B	C	D	E
20030209	18.079	0.174	0.816	0.431	2.105
20030210	18.036	0.173	0.818	0.429	2.104
20030215	16.574	0.432	0.259	0.805	2.049
20030216	13.784	0.805	0.156	0.478	1.687

We have near-IR photometry for 589 stars. In Table 11 we list the number of each star, their RA and DEC coordinates in J2000, and the value of J , H and K_S with the photometric error for each magnitude. There is only one measurement for each filter. The completeness limits in the 2MASS standard system are $J \sim 18$, $H \sim 17$ and $K_S \sim 18$.

Astrometric referencing of our images was made using positions of a number of stars from the 2MASS catalog. The PSFs of these stars are not corrupted by the CCD oversaturation effects. We used IRAF tasks `ccmap/cctran` for the astrometric transformation of the image. Formal rms uncertainties of the astrometric fit for our images are $< 0''.10$ in both right ascension and declination.

2.3 Spectroscopy

Spectra of the brightest stars in the area were taken with the *Aurélie* spectrograph on the 1.52-m telescope at the Observatoire de Haute Provence (OHP) during two dedicated runs on 2002 January 18–22 and 2002 February 25–28 (when only the first night was useful because of the weather). The spectrograph was equipped with grating #3 (600 ln mm^{-1}) and the Horizon 2000 2048×1024 EEV CCD camera (see Gillet et al. 1994 for a description of the instrument). In the classification region, this configuration gives a dispersion of 0.22 \AA/pixel (resolving power of approximately 7000), covering a wavelength range of $\approx 440 \text{ \AA}$. It is, therefore, necessary to observe two wavelength regions to cover the classical classification region.

For this programme, the two regions selected (identified as Position 1 and 2 in Table 5) were centred at $\lambda = 4175 \text{ \AA}$ and $\lambda = 4680 \text{ \AA}$. In principle, all objects were intended to

be observed in both regions, resulting in coverage in the $\lambda 3950 - 4900 \text{ \AA}$ range, with a small gap ($\sim 60 \text{ \AA}$) around $\lambda 4425 \text{ \AA}$. No strong photospheric lines are found in the gap, but the strong diffuse interstellar line (DIB) at $\lambda 4428 \text{ \AA}$, which is a good indicator of the reddening, is lost. The complete log of observations at the 1.52-m OHP is given in Table 5.

These spectroscopic data were reduced with the *Starlink* packages `CCDPACK` (Draper et al. 2000) and `FIGARO` (Shortridge et al. 1997) and analyzed using `FIGARO` and `DIPSO` (Howarth et al. 1998).

We took more spectra with the 2.6-m Nordic Optical Telescope (NOT, La Palma, Spain) on the nights of 2011 September, 1–2. The telescope was equipped with the imager and spectrograph Andalucía Faint Object Spectrograph and Camera (ALFOSC). Spectra of some of the brightest stars in Stock 8, Alicante 11 and Alicante 12 were obtained with ALFOSC. In spectroscopic mode, we used the grism #16 combined with a $1''$ slit to obtain intermediate resolution spectroscopy. Grism #16 covers the $3500 - 5060 \text{ \AA}$ range with a nominal dispersion of 0.8 \AA/pixel . The resolving power for this configuration is $R \sim 1000$. The log of observations at the NOT is given in Table 6.

These spectroscopic data were reduced using IRAF routines for the bias and flat-field corrections. The extraction of the spectra was done using the `APALL` package inside `APEXTRACT` in `TWODSPEC`. Once we had the spectra of targets and arcs, we used the package `IDENTIFY` to perform the wavelength calibration. We used ThAr arc lamp spectra, taken between the exposures. The rms for the wavelength solution is ≈ 0.2 pixels.

3 RESULTS

3.1 Spectral classification

To characterize the morphology of the whole region, we observed spectroscopically almost all the stars in the area that have been classified as early-type stars in the literature. The stars observed cover a region of approximately $40' \times 40'$ that includes the 3 open clusters studied and a very significant diffuse population scattered over most of the region. These stars are represented by open red squares in Fig. 1 and listed

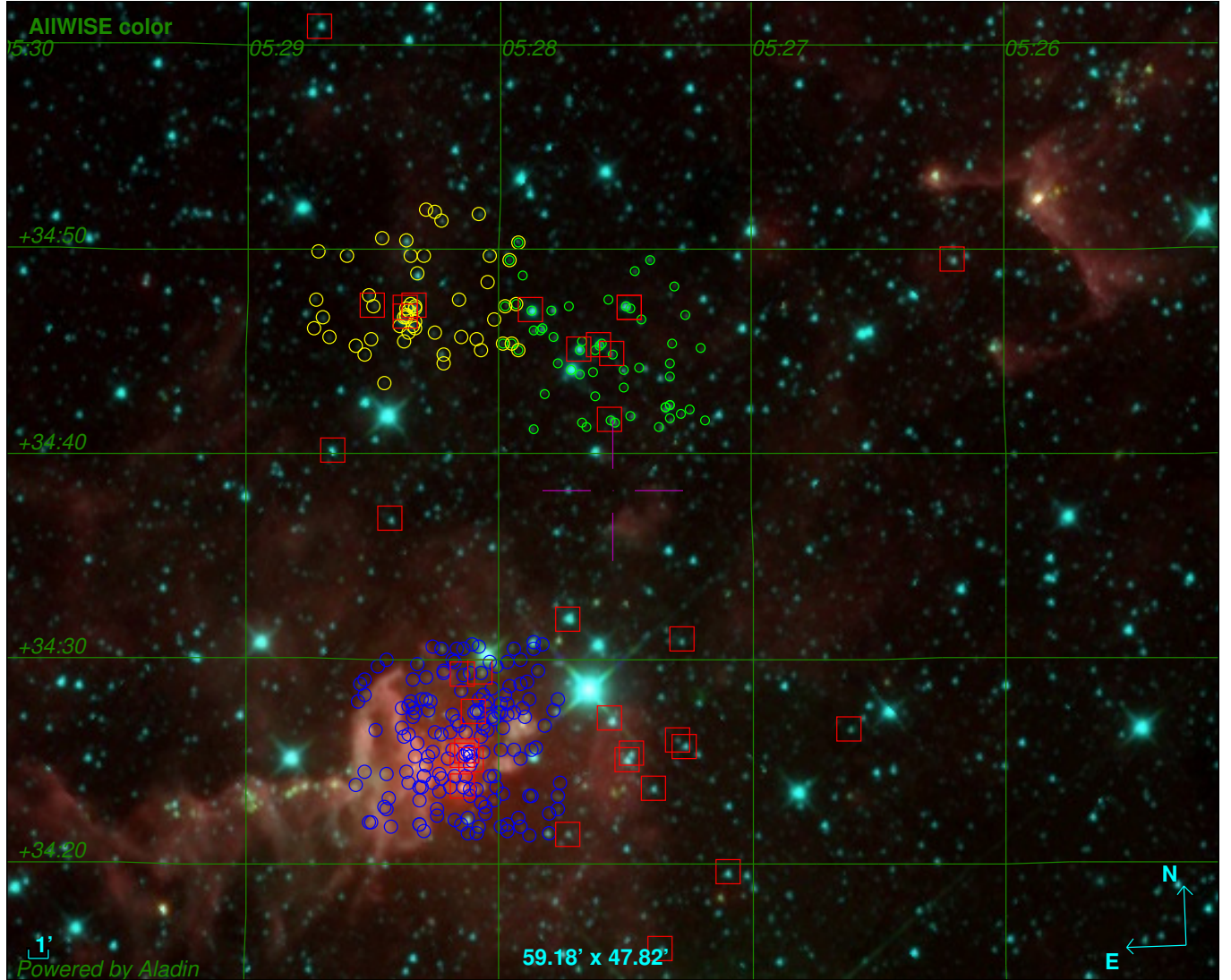


Figure 1. Map of the area showing the full field studied and the three areas for which we obtained Strömgren photometry. The image has been downloaded with Aladin and represents a false-colour composite of WISE bands. The pinkish regions represent extended dust emission. Red squares indicate stars with spectra. Circles in blue, green and yellow are stars with optical photometry in the three areas (Stock 8, Alicante 11 and Alicante 12). The Nebulous Stream of Jose et al. (2008) can be seen just to the east of Stock 8. The cluster candidate CC 14 is the small clump of infrared sources located where the stream meets the grid line corresponding to R.A. = 05h 29m. The size of field is $59'.18 \times 47'.82$. North is up and east is left.

in Tables 5 and 6. In these tables all the stars are listed by their identifier in the LS V (Hardorp et al. 1965) catalog except for HD 281147, which is missing in this catalog. Cross-correlation with our numbering system is provided for stars with photometry. Other more usual identifiers of the brightest stars, such as HD numbers, are also given.

The stars observed, according to their distribution, can be grouped as follows:

- The two brightest stars illuminating the H II region, at the core of Stock 8, LS V +34°29 (ST93) and LS V +34°31 (ST120), and a set of 5 stars within the limits given for Stock 8 by Jose et al. (2008): ST23, ST25, ST61, ST97 and ST101
- A group of 12 stars spread to the west of Stock 8 that have been assumed to be somehow connected to Stock 8 by previous authors: LS V +34°23, LS V +34°12, LS V +34°21,

LS V +34°13, LS V +34°14, LS V +34°11, LS V +34°16, LS V +34°18, LS V +34°15, LS V +34°24, LS V +34°10 and LS V +34°8

- Two stars to the north of Stock 8, clearly detached from the cluster, LS V +34°35 and LS V +34°36
- A more distant star to the north of Alicante 12: LS V +34°37
- Four stars in the core of Alicante 12: 20, 21, 24 and 30
- Six stars in the core of Alicante 11: 12, 27, 29, 49, 56 and 57

The spectra obtained were used for spectral classification by comparison to spectra of MK standard stars observed at similar resolution, following the standard classification procedures of Walborn & Fitzpatrick (1990). In a second step, we checked internal consistency by comparing all the spectra obtained amongst themselves. In principle, the much

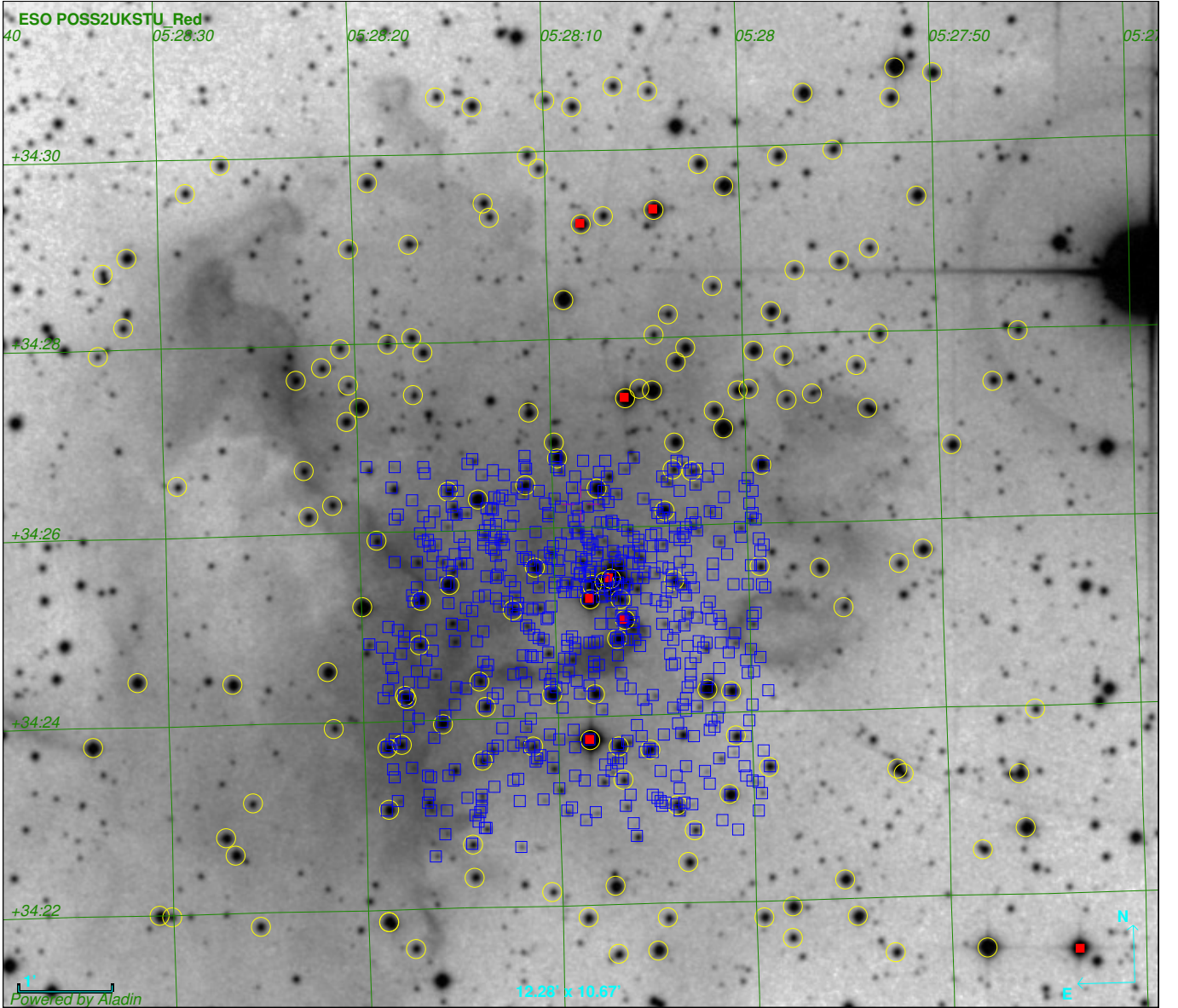


Figure 2. Finding chart for stars with photometry in the cluster Stock 8. The image, downloaded from Aladin, is a DSS2 red digitization. The dark areas thus map nebular $H\alpha$ emission. Red solid squares represent stars with spectra. Circles in yellow are stars with optical photometry and blue rectangles are stars with TNG near-IR photometry. Numbers and coordinates in J(2000) are listed in Tables 10 and 11. The size of field is $12'.28 \times 10'.67$. North is up and east is left.

higher resolution of the OHP spectra allows a much more accurate classification, but in some cases the signal-to-noise ratio in the $4000 - 4500 \text{ \AA}$ region is very low, resulting in inaccurate classifications, marked as such in Table 5. Spectra observed with ALFOSC can be considered accurate to ± 1 subtype.

All the stars in the LS catalog (Hardorp et al. 1965), as expected, turn out to be of early type. The only object that does not belong to the OB group is LSV +34°8 that, at B4III, is a bit too late for the catalog, and too old to belong to the same population as the rest of the stars in the region, even though its DM (calculated from the 2MASS data) is readily compatible. All the stars observed within the clusters have spectral types compatible with membership except for two early-type foreground objects, ST101 in Stock 8, and

Alicante 11-27. Noteworthy aspects of some of the spectra are discussed below:

- LSV +34°29 (ST 93) is the brightest star in Stock 8. The spectrum suggests it is a moderately fast rotator, but the lines appear very shallow (Fig. 5). Formally, the criterion $\text{Si III } 4553\text{\AA} \approx \text{He II } 4542\text{\AA}$ defines spectral type O9.7. The relative weakness of $\text{He II } 4686\text{\AA}$ indicates then a luminosity class IV. However, the Si IV lines are quite weak ($\text{Si IV } 4116\text{\AA}$ is not even seen). All metallic lines look too weak and shallow, and this suggests that this object is really a spectroscopic binary whose spectral type results from the combination of a late-O and an early-B star.

- LSV +34°23 has a spectral type O8, rather earlier than previously assigned (Fig. 5). It had been classified as B0.5IV by Morgan et al. (1953), most likely as a consequence of

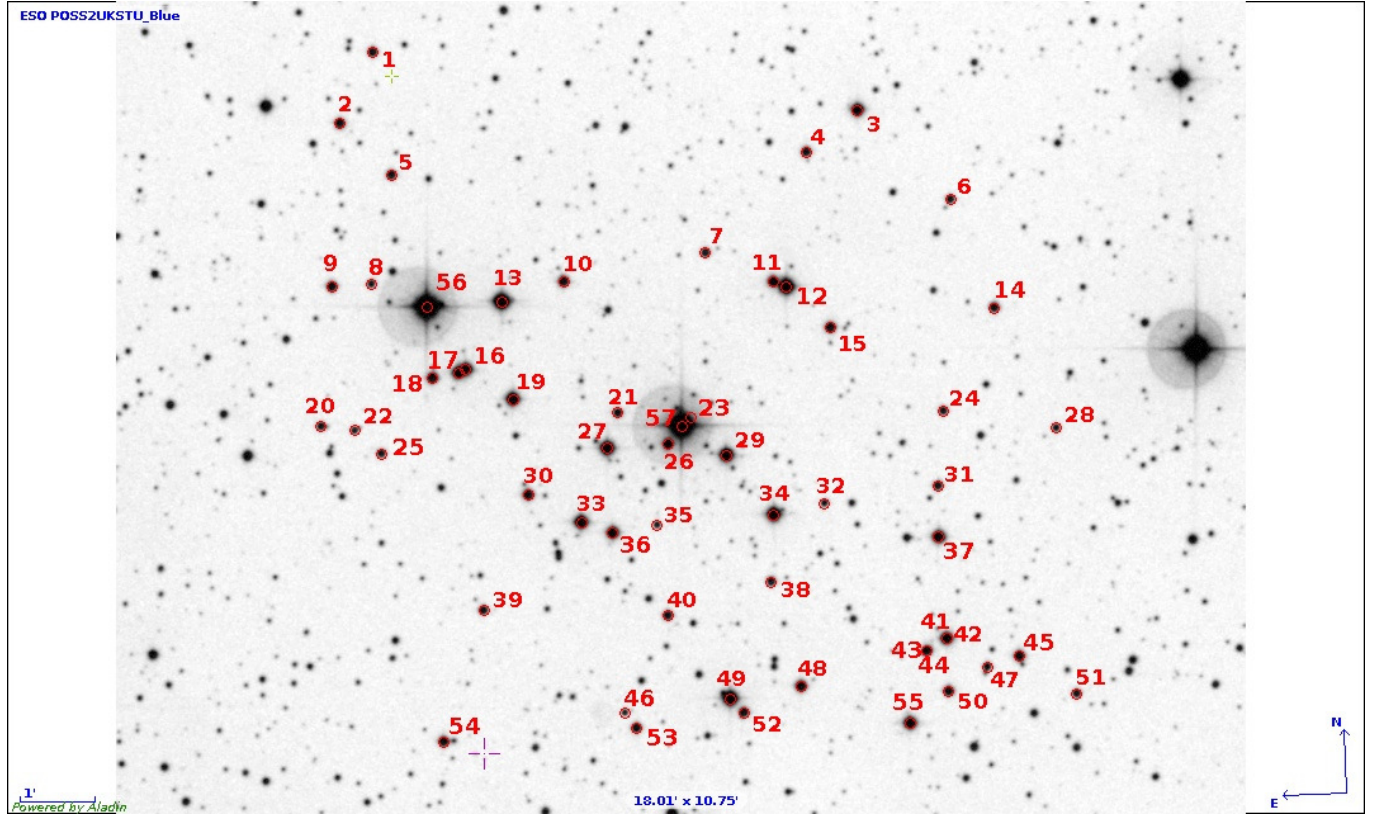


Figure 3. Finding chart for stars with photometry in Alicante 11. The image, provided by Aladin, is a DSS2 blue digitization. Numbers and coordinates in J(2000) are listed in Table 13. The size of the field is $18'01'' \times 10'75''$. North is up and east is left.

Table 5. Stars observed from the OHP 1.52-m. The first column indicates the volume and number in the Luminous Stars catalog or the name in the Henry Draper Catalog. The second and third columns indicate the dates when the two spectral positions were observed and (between brackets) the exposure time in seconds. The derived spectral types are given in the fourth column. Spectral types marked with a '*' are less secure than the average, because of poor signal to noise or presence of double lines. References for the photometric values in column 7 are: (1) Hiltner (1956) and (2) Mayer & Macak (1971).

Name Number	Position 1	Position 2	Spectral Type	V	(B - V)	Reference	DM ± 0.5	K _S
LSV +34°22 ¹	18/01 (600)	19/01 (700)	O7.5 V	8.58	0.23	2	11.5	7.89 ± 0.02
LSV +34°15	18/01 (750)	19/01 (900)	B1 V	10.02 ± 0.05	0.20	1	11.6	9.37 ± 0.02
LSV +34°16	18/01 (1000)	19/01 (1000)	B1 V*	–	–	–	–	9.22 ± 0.02
LSV +34°18	18/01 (750)	19/01 (1200)	O9.5 V*	10.01	0.67	2	11.0	8.04 ± 0.02
LSV +34°21	18/01 (1200)	19/01 (1500)	O9 V*	10.70	0.94	2	10.9	7.88 ± 0.02
LSV +34°29 ²	20/01 (1000)	25/02 (1200)	O9.7 IV	8.89	0.18	2	12.0	8.32 ± 0.02
LSV +34°31 ³	20/01 (1200)	25/02 (1200)	B0.5 V*	9.87	0.19	2	12.0	9.23 ± 0.02
LSV +34°36 ⁴	18/01 (600)	19/01 (750)	O8 V(n)	8.78	0.26	1	11.4	8.02 ± 0.03
LSV +34°23 ⁵	20/01 (750)	25/02 (900)	O8 II(f)	8.04	0.32	1	12.0	6.99 ± 0.02
LSV +34°25 ⁶	20/01 (750)	25/02 (1200)	O9.5 V + B0.2 V	–	–	–	–	7.59 ± 0.02
LSV +34°11 ⁷	18/01 (900)	19/01 (750)	B0.5 V	9.70	0.17	2	11.9	9.27 ± 0.02
HD 281147	18/01 (900)	19/01 (1200)	B1 V	–	–	–	–	9.63 ± 0.02

¹ HD 35619 = Alicante 11-57; ² BD +34°1054 = ST93; ³ BD +34°1056 = ST120; ⁴ BD +34°1058; ⁵ HD 35633; ⁶ HD 35652 = Alicante 11-56 (Eclipsing binary IU Aur); ⁷ HD 281150

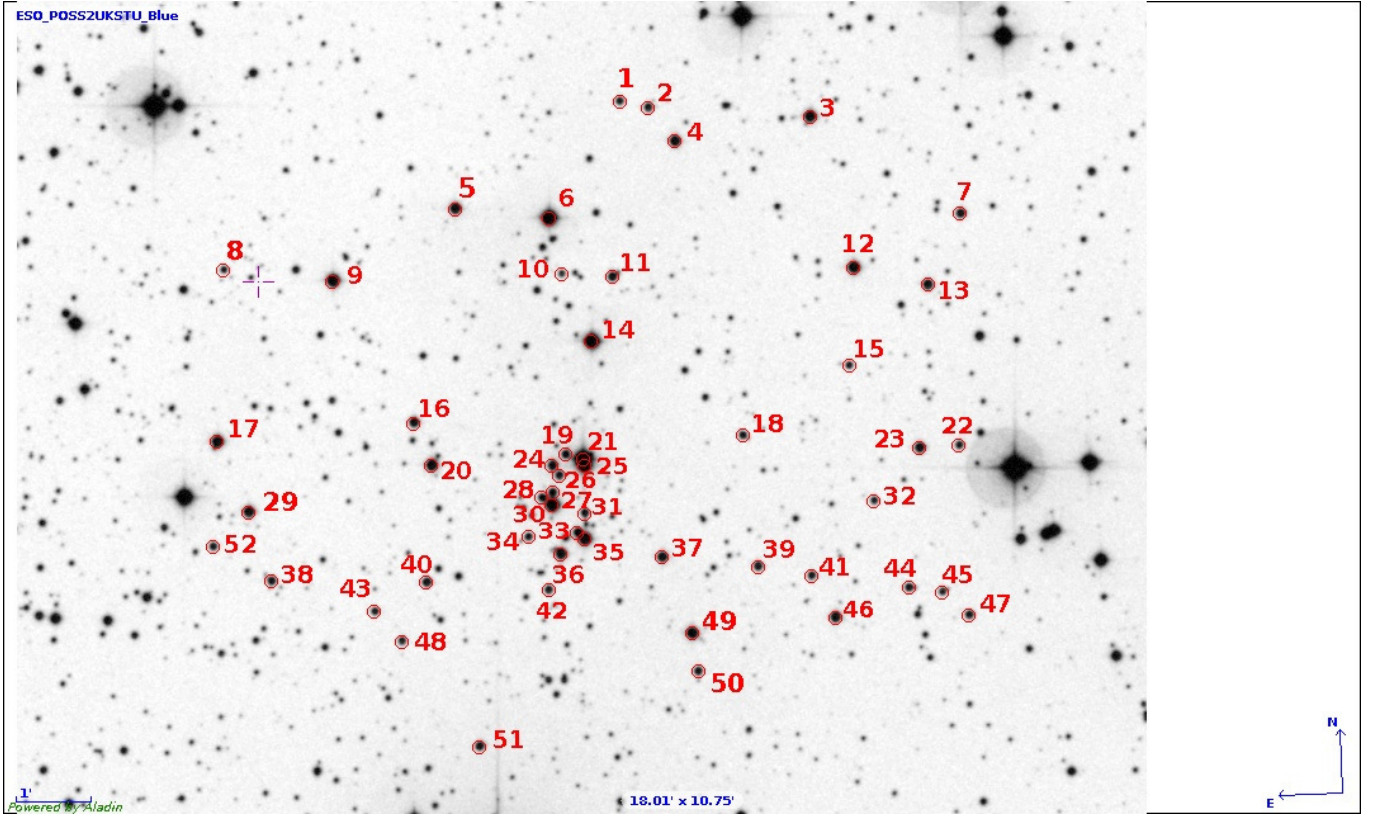


Figure 4. Finding chart for stars with photometry in Alicante 12. The image, provided by Aladin, is a DSS2 blue digitization. Numbers and coordinates in J(2000) are listed in Table 15. The size of field is $18'.01 \times 10'.75$. North is up and east is left.

Table 6. Classification spectra of stars in the area of Stock 8. These stars were observed with the NOT. References for the photometric values in column 7 are: (2) Mayer & Macak (1971) and (3) Mayer (1964).

Star	LS	Spectral Type	Exposure Time(s)	V	(B-V)	Reference	DM ± 0.5	K_S
Alicante 11-12	V +34°17	B2 V	250	–	–	–	–	10.16 ± 0.02
Alicante 12-21	V +34°33	B2 V	300	–	–	–	–	9.66 ± 0.03
Alicante 12-24	–	B7 V	300	–	–	–	–	12.82 ± 0.03
Alicante 12-20	–	B9 V	300	–	–	–	–	11.81 ± 0.02
Alicante 11-29	V +34°19	B2 V	400	–	–	–	–	10.77 ± 0.02
Alicante 11-49	V +34°20	B1.5 V	400	–	–	–	–	10.29 ± 0.02
–	V +34°14	B1 V	300	–	–	–	–	10.19 ± 0.02
ST101	–	A3 V	400	–	–	–	–	11.39 ± 0.01
ST97	V +34°30	B1 V	400	–	–	–	–	10.45 ± 0.02
ST61	V +34°28 ¹	B1 V	350	10.92	0.27	3	12.3	10.03 ± 0.02
ST23	V +34°27	B2 IV	400	11.66	0.33	3	13.0	10.70 ± 0.02
ST25	–	B5 V	400	–	–	–	–	11.63 ± 0.02
–	V +34°35	B0.7 V	200	–	–	–	–	9.75 ± 0.02
–	V +34°12	B1 V	300	10.91	0.30	2	12.2	10.01 ± 0.02
–	V +34°13	B2 IV	400	–	–	–	–	10.92 ± 0.02
Alicante 11-27	–	B8 V	300	–	–	–	–	8.06 ± 0.03
Alicante 12-30	–	B2 V	400	–	–	–	–	10.69 ± 0.02
–	V +34°8	B4 III	300	–	–	–	–	10.57 ± 0.02
–	V +34°24	B1 V	350	11.24	0.40	3	12.2	10.05 ± 0.02
–	V +34°10 ²	B0.2 V	200	9.43	0.16	2	11.7	9.01 ± 0.02
–	V +34°37 ³	O9.7 V	200	9.22	0.19	2	11.5	8.80 ± 0.02

¹ BD +34°1053; ² HD 281151; ³ BD +34°1059

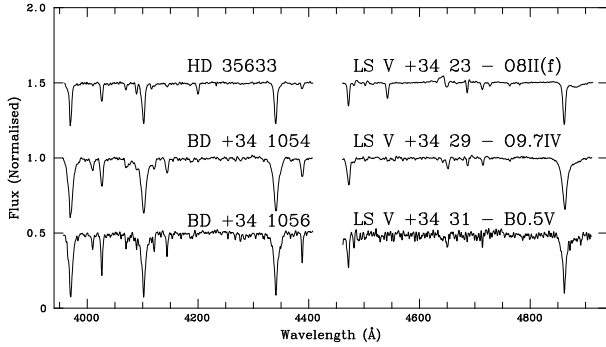


Figure 5. OHP spectra of the two brightest stars in Stock 8, and the nearby HD 35633 that is, very likely, the main source of ionization in IC 417. The small gap is due to the two different settings explained in the text.

misidentification. The N III 4634–41–42 complex is in emission, while He II $\lambda 4686\text{\AA}$ is very weak and flanked by emission components. The object, therefore, presents a rather high luminosity. Just short of being a supergiant according to the criteria of Sota et al. (2011), we classify it as O8 II(f), while noting the complete absence of any absorption N III lines. If the star is nitrogen deficient, it could probably have a higher luminosity.

- LS V +34°25 (Alicante 11-56) is a well known spectroscopic binary (IU Aur), which has received several very discrepant classifications. Though the two components are not very well resolved in the Position 1 spectrum, they are clearly separated in the Position 2 one (Fig. 6), and we derive spectral types of O9.5 V and approximately B0.2 V for the two components, based mainly on the relative strengths of the He II 4686 \AA and C III 4650 \AA lines. These values are in surprisingly good agreement with the masses $M_1 = 21.3 M_\odot$ and $M_2 = 14.4 M_\odot$ derived by Drechsel et al. (1994). Drechsel et al. (1994) also identify a third body in this system, with a mass $M_2 = 17.8 M_\odot$, which accounts for $\sim 20\%$ of the light. Since a third spectrum is not seen, Drechsel et al. (1994) support the idea that the third body is a close binary consisting of two B2–B3 stars.

- LSV +34°22 (Alicante 11-57) is the brightest star in Alicante 11. Based on standard criteria, we classify it as O7.5 V. Sota et al. (2014) give a more accurate classification O7.5 V((f)z), based on higher-quality spectra.

- LS V +34°36, classified as O8nn by Morgan et al. (1955) does not show very broad lines in our spectrum (Fig. 6). The object, though, is a double-lined spectroscopic binary. The combined spectrum has spectral type O8 V, but all the lines are broad and asymmetric, clearly showing the presence of a second companion. Given the width of He II 4542 \AA , the two components are O-type stars. Since He II 4686 \AA is abnormally weak, at least one of them could be of higher luminosity.

- HD 281147 is given as O8nn in Simbad, after Garmany & Conti (1984). This is almost certainly due to a confusion with BD +34°1058, which is the object observed by *IUE*. Our spectrum gives a spectral type B1 V.

- The Position 1 spectra of LS V +34°16, LS V +34°18, and LSV +34°21 are little more than noise, and therefore their spectral types are based on a very limited spectral range, and must not be considered accurate.

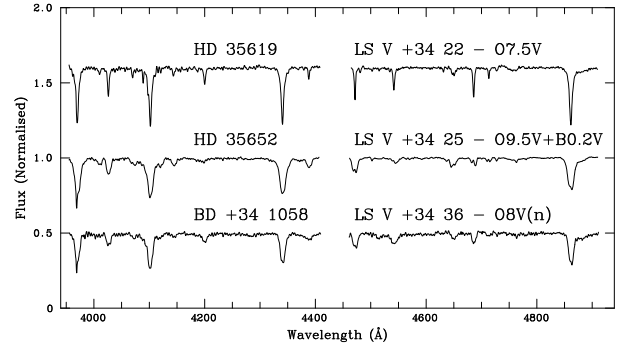


Figure 6. OHP spectra of other O-type stars in the area. HD 35619 and HD 35652 are part of Alicante 11. BD +34°1058 lies north of Stock 8.

The distribution of spectral types in the region is shown in Fig 17. No obvious pattern emerges.

3.2 HR diagrams

3.2.1 Optical photometry for Stock 8

As a first step, we analyzed the *uvby* β CCD photometry obtained for the cluster Stock 8 (Table 12) to determine the physical parameters of the cluster: reddening, distance and age. Initially, we plotted the diagrams $V/(b-y)$ and V/c_1 for all the stars in the field. In Fig. 7 red circles are stars with spectra and green squares are stars that appear misplaced in both diagrams and, therefore, were removed for the following analysis.

The next step in the analysis is the estimate of membership for the stars measured in the field. Given the depth of our observations, and the presence of O-type stars confirmed by spectroscopy, most cluster members in our sample must be B-type stars. Now, we can calculate the reddening-free indices $[m_1]$, $[c_1]$ and $[u-b]$, where:

$$[m_1] = m_1 + 0.32(b-y) \quad (6)$$

$$[c_1] = c_1 - 0.20(b-y) \quad (7)$$

$$[u-b] = [c_1] + 2[m_1] \quad (8)$$

We plot the $[c_1]$ - $[m_1]$ and β - $[u-b]$ diagrams for all stars chosen in the V - $(b-y)$ and V - c_1 diagrams (see Fig. 8). We can divide the stars according to their spectral type. In this figure we can see that the stars spectroscopically classified (red squares) as B-type stars fall on the B-type star standard line, confirming the validity of this relationship. The only star classified as A3 V falls on the A-type star standard line. We can observe that the majority of the stars are in the same region in both diagrams. Therefore, using these standard relationships, we assign a spectral type for each star. After this, we use those stars falling on the B-type branch in both diagrams to make the following analysis.

Firstly, we calculate individual reddenings. We follow the procedure described by Crawford et al. (1970b): we use the observed c_1 to predict the first approximation to $(b-y)_0$ with the expression: $(b-y)_0 = -0.116 + 0.097c_1$. Then we calculate: $E(b-y) = (b-y) - (b-y)_0$ and use $E(c_1) = 0.2E(b-y)$ to correct c_1 for reddening $c_0 = c_1 - E(c_1)$. The intrinsic colour $(b-y)_0$ is now calculated by replacing c_1 with c_0 in the above

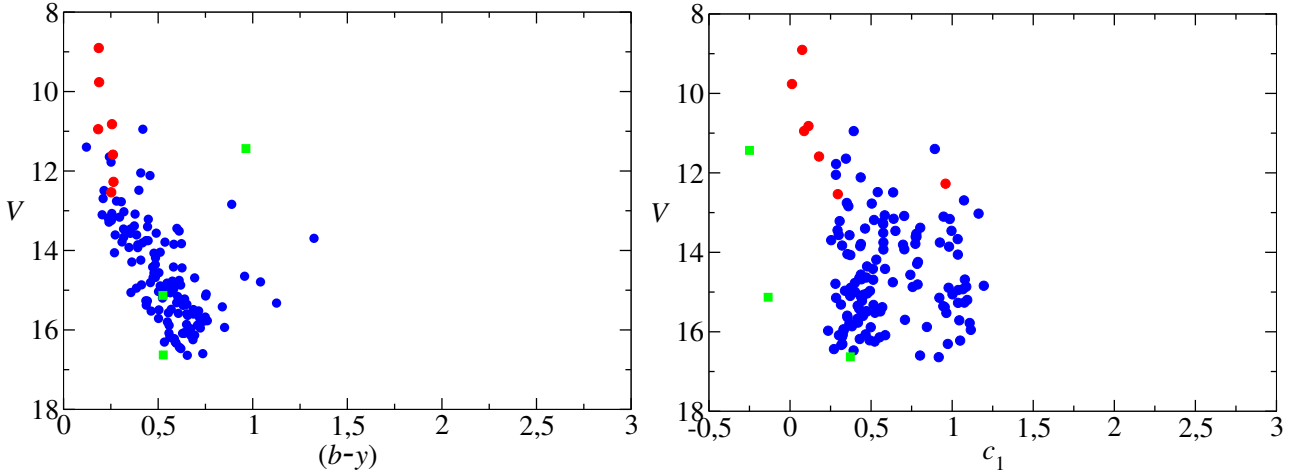


Figure 7. *Left:* $V/(b-y)$ diagram for all stars in Stock 8. Red circles represent stars spectroscopically observed and green squares, non-member stars. *Right:* V/c_1 diagram for all stars in Stock 8. Red circles represent stars spectroscopically observed and green squares non-member stars.

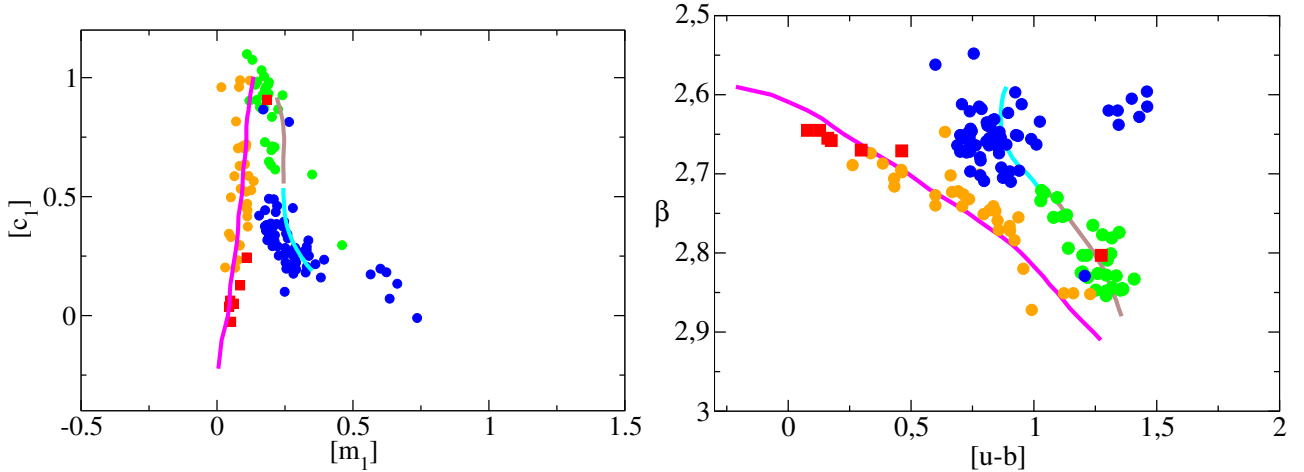


Figure 8. *Left:* The $[c_1]-[m_1]$ diagram for the stars observed in the open cluster Stock 8. The solid lines represent the average loci of field B-type (magenta line), A-type (brown line) and F-type (cyan line) main-sequence stars (Perry et al. 1987). *Right:* The $\beta-[u-b]$ diagram for the stars observed in the open cluster Stock 8. The colour convention is as in the left panel, with the average loci of field stars also taken from Perry et al. (1987). In both diagrams, red squares correspond to spectroscopically observed stars. Orange circles are stars falling close to the position of B-type stars in the two diagrams; green dots are A-type stars, and blue dots are identified as F-type stars

equation for $(b-y)_0$. Three iterations are enough to reach convergence in the process. Naturally, this procedure only results in physically meaningful values for B-type stars. As we can see in the maps (see Fig. 1 and Fig. 2), the area of Stock 8 is still embedded in the parental cloud and therefore we expect to find an important degree of differential reddening amongst members. $E(b-y)$ spans values between 0.3 and 0.8. In Fig. 9 we plot their surface distribution that can be compared with the extent of the cloud. Most of the stars with relatively low reddening (marked in red) fall along a narrow strip, almost vertical, that seems to coincide with a gap in the dark cloud. Stars with higher reddening concentrate almost exclusively close to the illuminated rim of the cloud.

With the aid of these individual values, we calculate the intrinsic colour $(b-y)_0$, index c_0 , and magnitude V_0 of the

38 likely B-type members. The values of $E(b-y)$, c_0 and V_0 for these likely B-type members are shown in Table 7.

3.2.2 Determination of the distance for Stock 8

We estimate the DM to Stock 8 by fitting the observed V_0 vs. $(b-y)_0$ zero-age main sequence (ZAMS) and V_0 vs. c_0 ZAMS to the mean calibrations of Perry et al. (1987). We fit the ZAMS as a lower envelope for the majority of members, deriving a best fit distance modulus of $V_0 - M_V = 12.2 \pm 0.2$ (the error indicates the uncertainty in positioning the theoretical ZAMS and its identification as a lower envelope; see Fig 10). This DM corresponds to a distance of $2.80^{+0.27}_{-0.24}$ kpc.

We can check the validity of the distance modulus adopted by eye fitting, by comparing the absolute magnitude M_V obtained for the stars with spectral classification

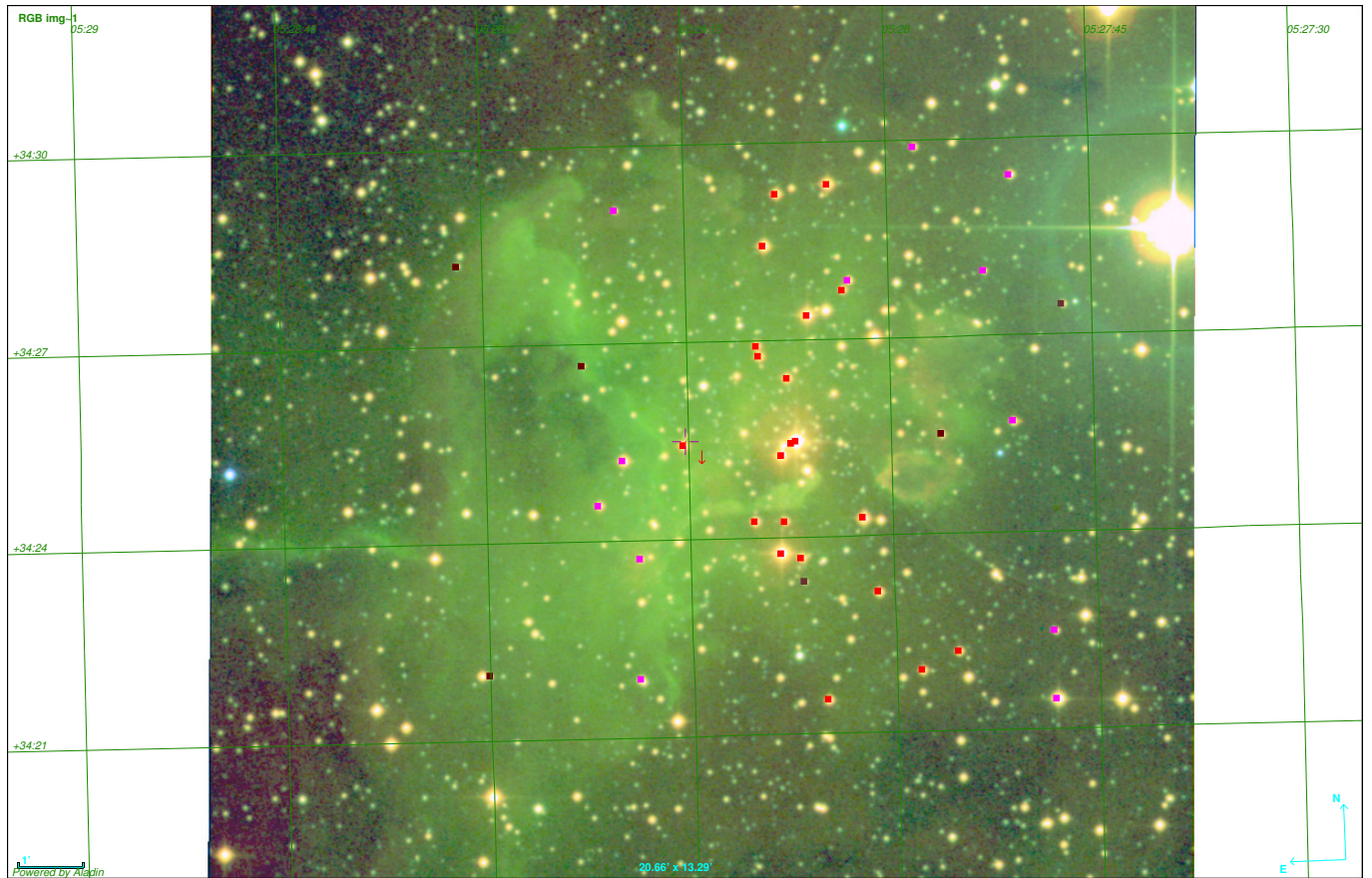


Figure 9. Reddening map for B-type stars with optical photometry in the cluster Stock 8. The image, downloaded from Aladin, is a false-colour composite of the three DDS bands, where R (and, hence $H\alpha$) is represented by green colours. Red solid squares represent stars with low reddening [$E(b-y) = 0.3-0.4$]. Pink solid squares are stars with moderately reddening [$E(b-y) = 0.5-0.6$] and black solid squares are stars with high reddening [$E(b-y) = 0.7-0.8$]. North is up and east is left.

and their values in the calibration from Turner (1980). We can say that all values are compatible within errors, except for the A3 V star that is considered a non-member.

3.2.3 Optical photometry for Alicante 11

We used the same procedure described in Sections 3.2.1 and 3.2.2 to analyze the photometric data from Table 14. Firstly, we plotted the $V/(b-y)$ and V/c_1 diagrams for stars in Alicante 11, where the red points are stars with spectra and green squares are stars that do not occupy the expected position in any of the diagrams. These outliers are considered field population and therefore, not used in the subsequent analysis (see Figure 11). Secondly, we selected B-type stars using the $[c_1]-[m_1]$ and $\beta-[u-b]$ diagrams. All the early-type stars spectroscopically classified fall on the correct position in both diagrams, except Alicante 11-27 (B8 V), that we consider a non-member. After this, using the procedure described by Crawford et al. (1970b), we calculated the individual reddenings $E(b-y)$ for 28 stars that we label as likely members. As seen in Figure 1 and Figure 3, the region of Alicante 11 is outside the gas and dust cloud that covers the area where Stock 8 lies. Because of this, stars in this region present rather lower values of reddening compared to those of Stock 8. Most of them have values of $E(b-y)$ around 0.4,

which is the same $E(b-y)$ that we found for the stars in Stock 8 falling along the narrow strip that seems to coincide with a gap in the dark cloud.

With the aid of these individual values, we calculated the intrinsic colour $(b-y)_0$, index c_0 and magnitude V_0 of the 28 likely B-type members. The values of $E(b-y)$, c_0 and V_0 for these likely members are shown in Table 8.

3.2.4 Determination of the distance for Alicante 11

We estimated the distance modulus to Alicante 11 by using the same procedure as for Stock 8. The fit of the ZAMS as a lower envelope for the majority of members in the V_0 .vs. $(b-y)_0$ and V_0 .vs. c_0 diagrams (see Fig 12) gives a distance modulus of $V_0 - M_V = 12.2 \pm 0.2$ ($2.80^{+0.27}_{-0.24}$ kpc). We can then check the validity of the distance modulus by comparing the absolute magnitude M_V obtained for the stars with spectral classification. All of them give values compatible within errors with the calibration of Turner (1980), except for the binary star IU Aur, which, as discussed above, is likely a complex system with no less than four OB stars. The absolute magnitude that we obtain for IU Aur assuming the distance to the cluster is totally compatible with the configuration outlined by Drechsel et al. (1994).

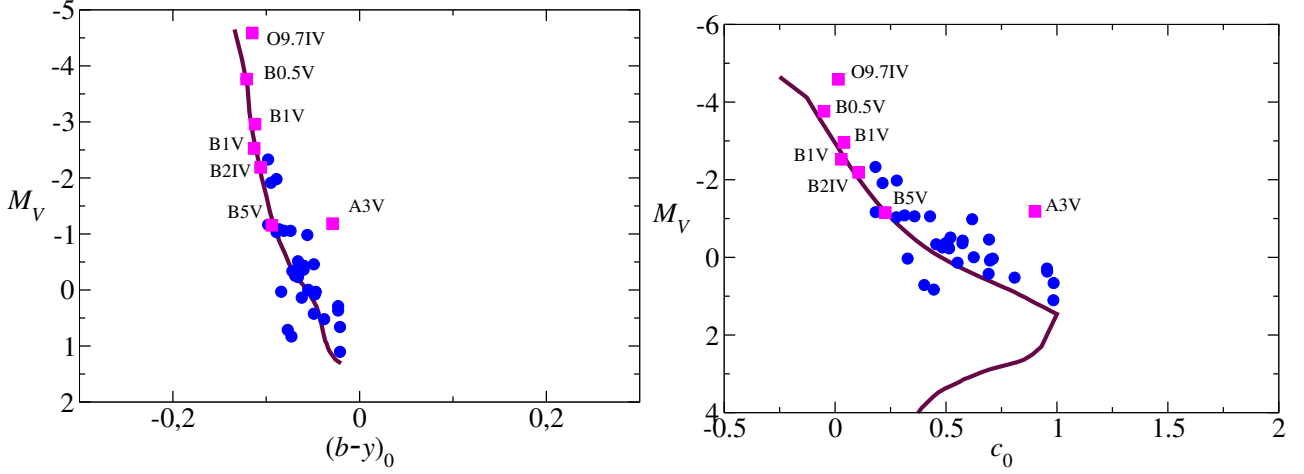


Figure 10. *Left:* Absolute magnitude M_V against intrinsic colour $(b-y)_0$ for Stock 8. Solid magenta squares are stars with spectra. The solid line represents the ZAMS from Perry et al. (1987). *Right:* Absolute magnitude M_V against intrinsic index c_0 for Stock 8. Solid magenta squares are stars with spectra. The solid line represents the ZAMS from Perry et al. (1987).

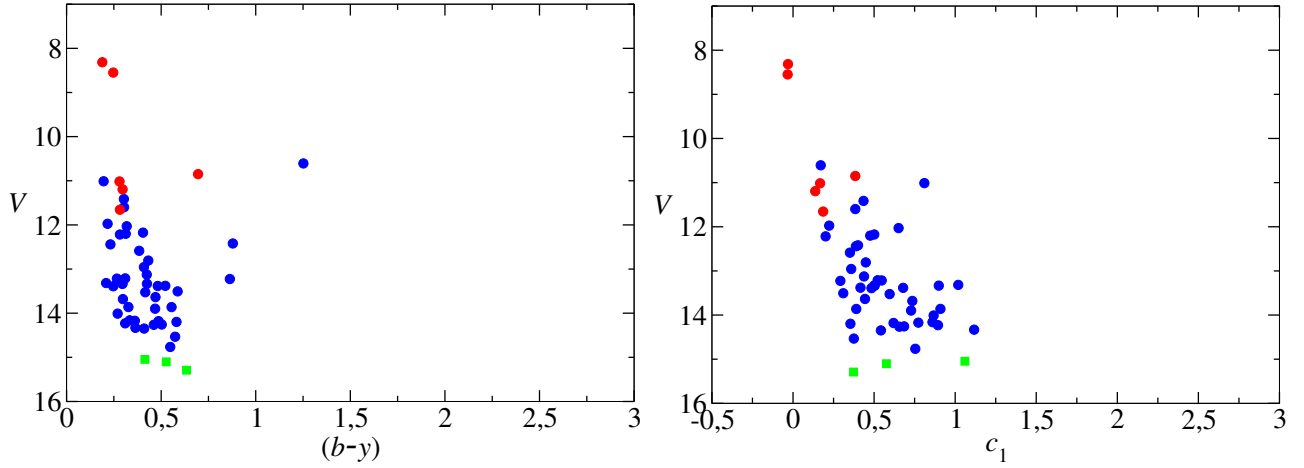


Figure 11. *Left:* $V/(b-y)$ diagram for all stars in Alicante 11. Red circles represent stars spectroscopically observed and green squares non-member stars. *Right:* V/c_1 diagram for all stars in Alicante 11. Red circles represent stars spectroscopically observed and green squares non-member stars.

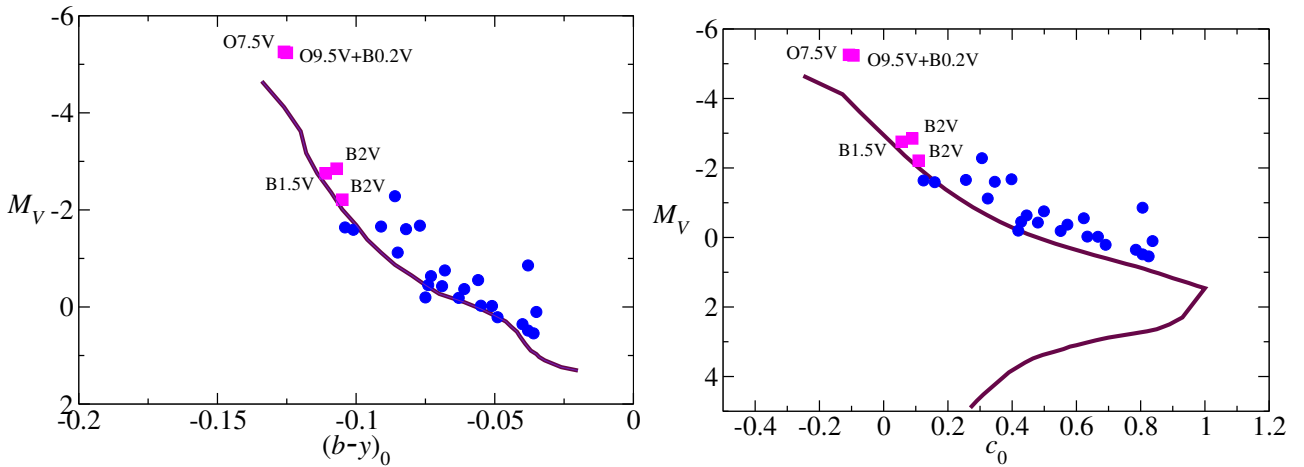


Figure 12. *Left:* Absolute magnitude M_V against intrinsic colour $(b-y)_0$ for Alicante 11. Solid magenta squares are stars with spectra. The solid line represents the ZAMS from Perry et al. (1987). *Right:* Absolute magnitude M_V against intrinsic index c_0 for Alicante 11. Solid magenta squares are stars with spectra. The solid line represents the ZAMS from Perry et al. (1987).

Table 7. Values of $E(b-y)$, c_0 , and V_0 for likely B-type members in Stock 8.

Star	$E(b-y)$	c_0	V_0
ST14	0.46	0.70	12.28
ST21	0.53	0.36	11.14
ST23	0.37	0.11	10.01
ST25	0.35	0.23	11.05
ST28	0.46	0.98	13.30
ST34	0.35	0.21	10.29
ST35	0.78	0.55	12.34
ST45	0.54	0.98	12.86
ST46	0.46	0.48	11.95
ST50	0.40	0.62	12.20
ST60	0.68	0.50	11.84
ST61	0.37	0.04	9.24
ST69	0.32	0.71	12.23
ST71	0.32	0.52	11.69
ST72	0.76	0.69	12.62
ST80	0.38	0.43	11.14
ST86	0.62	0.31	11.12
ST89	0.77	0.96	12.49
ST91	0.37	0.28	11.17
ST93	0.30	0.02	7.61
ST96	0.51	0.18	9.87
ST97	0.30	0.03	9.67
ST104	0.59	0.18	11.03
ST110	0.43	0.62	11.22
ST111	0.36	0.70	12.25
ST112	0.33	0.28	10.22
ST119	0.57	0.33	12.23
ST120	0.31	-0.05	8.44
ST124	0.32	0.51	11.87
ST128	0.71	0.45	13.03
ST134	0.32	0.58	11.77
ST142	0.55	0.96	12.57
ST146	0.43	0.69	11.74
ST148	0.75	0.40	12.91
ST151	0.56	0.81	12.72
ST152	0.38	0.57	11.84
ST159	0.31	0.46	11.86
ST163	0.31	0.51	11.97

3.2.5 Optical photometry for Alicante 12

We performed the same analysis done in Sections 3.2.1 and 3.2.2 for Stock 8 and Sections 3.2.3 and 3.2.4 for Alicante 11. We plot the $V/(b-y)$ and V/c_1 diagrams for stars in Alicante 12, where the red points are stars with spectra and green squares are stars considered non-members by applying the same criteria as in the other clusters (see Figure 13). We selected the B-type members from the $[c_1]$ - $[m_1]$ and β - $[u-b]$ diagrams, checking that their V values corresponded to their spectral types and, then, we calculated their individual $E(b-y)$. We find that the average value is $E(b-y) = 0.4$, similar to the value for the stars in Alicante 11. We can observe in Figure 1 and Figure 4 that the cluster is not inside the parental cloud. Finally, we calculate the dereddened values $(b-y)_0$, c_0 and V_0 of the 17 likely B-type members (displayed in Table 9).

Table 8. Values of $E(b-y)$, c_0 and V_0 for likely B-type members in Alicante 11.

Star	$E(b-y)$	c_0	V_0
Alicante 11-2	0.46	0.81	11.34
Alicante 11-3	0.39	0.40	10.52
Alicante 11-5	0.36	0.84	12.30
Alicante 11-6	0.56	0.57	11.83
Alicante 11-12	0.39	0.09	9.35
Alicante 11-15	0.37	0.43	11.75
Alicante 11-17	0.32	0.32	11.08
Alicante 11-19	0.32	0.16	10.61
Alicante 11-21	0.35	0.83	12.74
Alicante 11-22	0.60	0.63	12.17
Alicante 11-23	0.39	0.31	9.92
Alicante 11-25	0.52	0.55	12.01
Alicante 11-26	0.32	0.42	12.00
Alicante 11-29	0.39	0.11	9.99
Alicante 11-30	0.34	0.48	11.77
Alicante 11-31	0.52	0.62	11.65
Alicante 11-37	0.39	0.12	10.56
Alicante 11-38	0.41	0.69	12.41
Alicante 11-39	0.37	0.79	12.55
Alicante 11-40	0.31	0.81	12.69
Alicante 11-41	0.48	0.26	10.54
Alicante 11-42	0.48	0.50	11.45
Alicante 11-45	0.38	0.45	11.57
Alicante 11-48	0.51	0.35	10.60
Alicante 11-49	0.41	0.06	9.45
Alicante 11-53	0.35	0.67	12.18
Alicante 11-56	0.31	-0.09	6.96
Alicante 11-57	0.37	-0.11	6.94

Table 9. Values of $E(b-y)$, c_0 and V_0 for likely B-type members in Alicante 12

Star	$E(b-y)$	c_0	V_0
Alicante 12-3	0.46	0.13	10.75
Alicante 12-13	0.54	0.49	11.01
Alicante 12-21	0.35	-0.02	8.84
Alicante 12-24	0.32	0.74	12.60
Alicante 12-30	0.38	0.23	10.07
Alicante 12-31	0.38	0.86	12.93
Alicante 12-32	0.66	0.65	11.93
Alicante 12-33	0.42	0.68	12.23
Alicante 12-35	0.36	0.20	10.49
Alicante 12-36	0.39	0.25	11.26
Alicante 12-37	0.44	0.48	11.52
Alicante 12-40	0.33	0.79	12.66
Alicante 12-41	0.36	1.03	13.21
Alicante 12-42	0.37	0.99	13.04
Alicante 12-45	0.73	0.46	11.57
Alicante 12-46	0.40	0.50	11.69
Alicante 12-51	0.44	0.61	12.27

3.2.6 Determination of the distance for Alicante 12

As with the other two clusters, we estimated the distance modulus to Alicante 12 by fitting the ZAMS as a lower envelope in the dereddened photometric diagrams (see Fig 14). For this cluster, we also derive a best fit distance modulus of $V_0 - M_V = 12.2 \pm 0.2$ ($2.80^{+0.27}_{-0.24}$ kpc). Again, we can check the validity of the distance modulus, by comparing the ab-

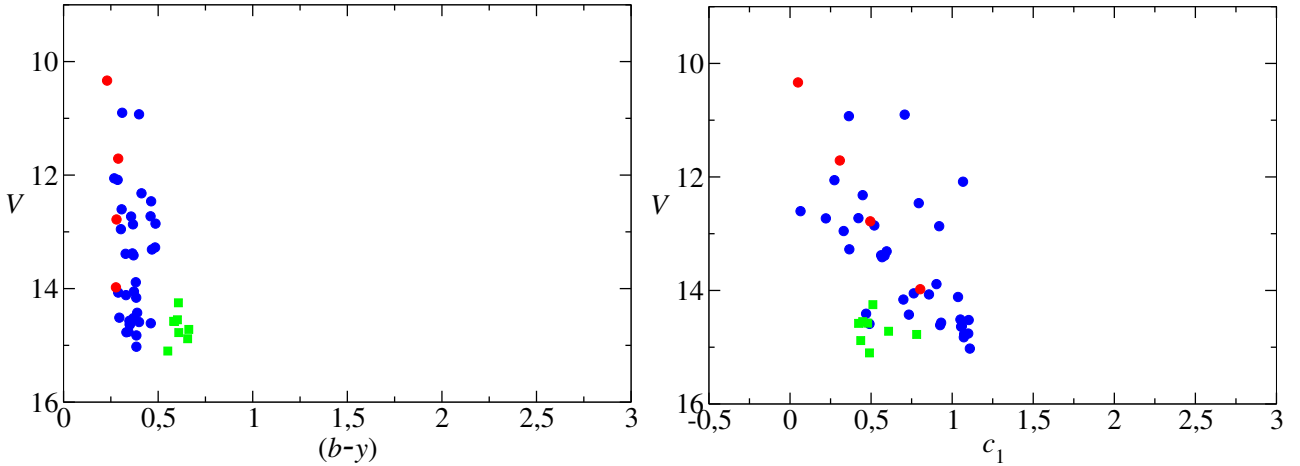


Figure 13. *Left:* $V/(b-y)$ diagram for all stars in Alicante 12. Red circles represent stars spectroscopically observed and green squares non-member stars. *Right:* V/c_1 diagram for all stars in Alicante 12. Red circles represent stars spectroscopically observed and green squares non-member stars.

solute magnitude M_V obtained for the stars with spectral classification to the calibration of Turner (1980). All stars are compatible within errors, except for the star classified as B9 V that we do not consider a member.

3.2.7 A common distance for Stock 8, Alicante 11 and Alicante 12

We have obtained optical photometry for the three different regions indicated in Figure 1. The first region corresponds to the known open cluster Stock 8 that is still partially embedded in its parental cloud. The two other regions are approximately $20'$ north of Stock 8 and not associated with the nebulosity. Strömgren photometry allows us to study the population of these three regions and to determine their distances with accuracy. We have calculated a distance for Stock 8 of $2.80^{+0.27}_{-0.24}$ kpc using 38 likely early type members. In the other two regions, we find clear sequences of early type stars that define two new clusters that had not been studied before, and we name Alicante 11 and Alicante 12. We have found 28 likely B-type members for Alicante 11 and 17 likely B-type members for Alicante 12, and we have estimated the same distance as for Stock 8. Their coordinates are shown in Table 1. The typical $E(b-y)$ values for B-type members in the two new clusters are very similar, and also similar to those found for the stars placed in a hole in the cloud surrounding Stock 8. This concordance suggests that the two new open clusters are fully detached from their parental cloud, and therefore, the reddening in their directions is entirely caused by intervening foreground material. In Figure 15, we plot the absolute magnitude M_V against intrinsic index c_0 for all the stars considered members in Stock 8 (blue), Alicante 11 (green) and Alicante 12 (cyan). Squares are stars with spectra. We can see that all of them are placed at the same distance modulus of $V_0 - M_V = 12.2 \pm 0.2$, corresponding to a distance of $2.80^{+0.27}_{-0.24}$ kpc

3.2.8 Bright stars with spectra. Determination of their distance modulus

In addition to the three open clusters, there is a large, diffuse population of OB stars scattered over the whole area. Many of them have UBV photometry available in the literature, and all of them have JHK_S photometry from 2MASS. We used their spectral types to calculate their distance moduli and check if they are compatible with the common DM that we find for Stock 8, Alicante 11 and Alicante 12 ($V_0 - M_V = 12.2 \pm 0.2$). For objects with UBV photometry, we utilized the calibration of intrinsic colours from Fitzgerald (1970) and the calibration of average absolute magnitude against spectral type from Turner (1980). The results are shown in Tables 5 and 6.

We find that essentially all the stars with UBV photometry have a distance modulus compatible within errors with the value obtained for the three open clusters studied. Generally, calibrations are assumed to have an intrinsic dispersion around ± 0.5 magnitudes. Possible exceptions would be LSV +34°18, LSV +34°21, and LSV +34°36. For the latter, we have already mentioned that the spectral type is simply the average of two components, one of which is likely more luminous, and so the discrepancy in DM is only apparent. The other two are marked as the less reliable spectral types, as their spectra are very poor. In many cases early-type stars are binaries or multiple systems, and then the spectral type derived from a single spectrum of moderate resolution can be an average of the spectral types of the components. Therefore, we do not think that any of these stars is ruled out as a member of the association, while LSV +34°36 is very likely a member, and one of the main sources of ionizing photons in the area.

For the stars without UBV photometry, we can use the $(J-K)_S$ colour to check that the extinction is not higher than that of members of Alicante 11 and 12, and the K_S magnitude to check that their brightness is not incompatible with its spectral type at the DM of the clusters. Thus, we can conclude that all of the isolated stars seen in the area are compatible with the common distance of all three clusters, and therefore they form an OB association extending over

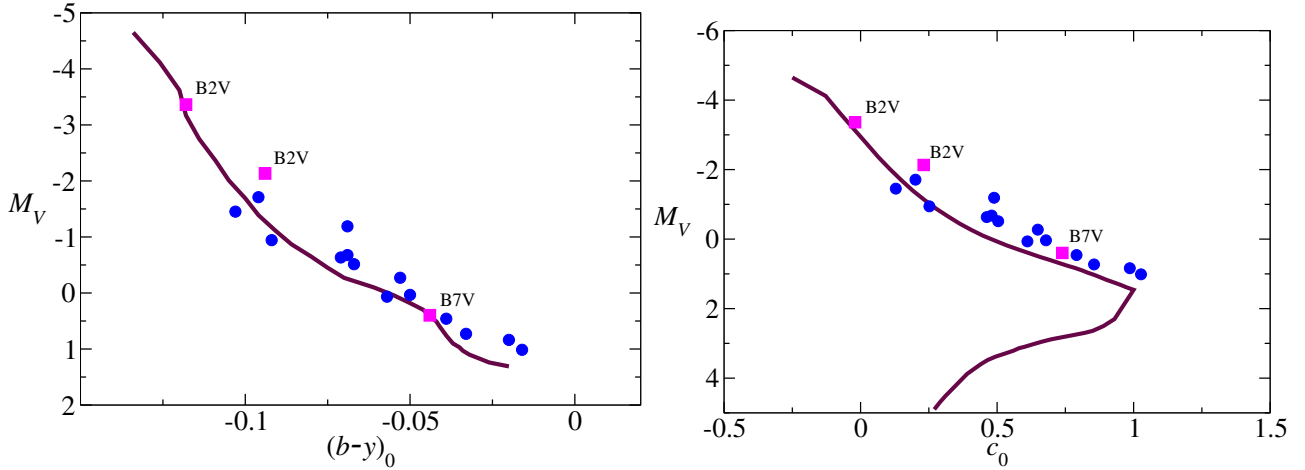


Figure 14. *Left:* Absolute magnitude M_V against intrinsic colour $(b-y)_0$ for Alicante 12. Solid magenta squares are stars with spectra. The solid line represents the ZAMS from Perry et al. (1987). *Right:* Absolute magnitude M_V against intrinsic index c_0 for Alicante 12. Solid magenta squares are stars with spectra. The solid line represents the ZAMS from Perry et al. (1987).

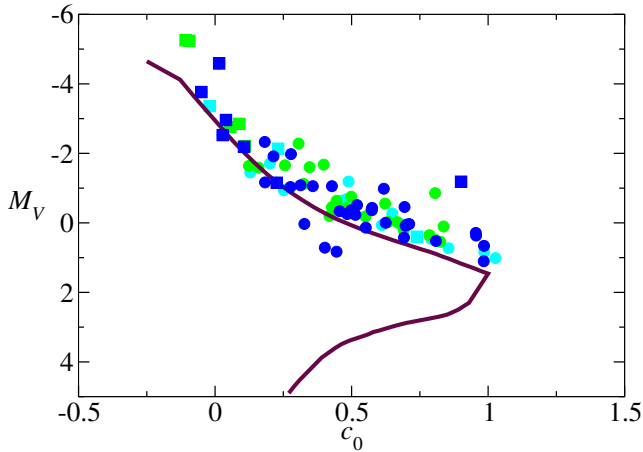


Figure 15. Absolute magnitude M_V against intrinsic index c_0 for Stock 8 (blue), Alicante 11 (green) and Alicante 12 (cyan). Squares are stars with spectra. The thick line represents the ZAMS from Perry et al. (1987).

at least the region studied, i.e., over $\sim 50'$ corresponding to ~ 40 pc at 2.80 kpc.

3.2.9 2MASS diagram

Most of the stars observed lie in areas completely devoid of not only $H\alpha$ nebulosity, but also dust emission (see Fig. 1). The obvious exception is the region of the open cluster Stock 8, which lies in a typical $H\text{II}$ “blister” on the wall of a molecular cloud (see Fig. 2). This area, as can be seen in Fig. 1, also shows strong dust emission. It is therefore important to use infrared wavelengths to detect and study the population hidden by nebulosity. To this purpose, we have used our own TNG near-IR photometry, combined with the 2MASS catalog (see Tables 10 and 11 for Stock 8).

Initially, we plot the K_S magnitude against the $(J-K_S)$ colour in Fig. 16. Since we have already determined a distance modulus of $V_0 - M_V = 12.2 \pm 0.2$ and a minimum $E(b-y) = 0.4$ with the optical photometry, we use these val-

ues to draw the ZAMS. We use isochrones from Siess et al. (2000) with $Z = 0.020$ and no overshooting. The ZAMS extends from spectral type M6 until B3. The PMS isochrones for ages 4×10^6 and 6×10^6 years are also plotted in Figure 16. We calculated $E(J-K_S) = 0.3$ using the standard relationships: $E(b-y) = 0.74E(B-V)$ and $E(J-K_S) = 0.476E(B-V) + 0.007(E(B-V))^2$. In Fig. 16, the likely B-type members (from the optical analysis) are represented as black solid circles, while the pink dots are stars with TNG photometry. We can observe that there is clearly a PMS star population associated with the B-type likely members. We can see a gap between K_S of 14 and 15 mag, where there are no stars and so we fit the PMS isochrones to the stars on the top of this gap. From their position, we conclude that all the PMS stars formed in a single process of star formation between 4×10^6 and 6×10^6 years ago. We have no stars already leaving the upper-main sequence (because of evolution) and, therefore, we cannot use post-main-sequence isochrones to estimate the age of the cluster. Taking into account the position of the PMS isochrones, we can interpret that the pink dots with $(J-K_S) < 1$ are foreground stars and the rest of the stars are the PMS population of the cluster together with some field contamination that we estimate below.

To characterize some properties of the PMS stars in Stock 8, we used the Wide-field Infrared Survey Explorer (WISE) catalog (Wright et al. 2010; Jarrett et al. 2011). WISE mapped the entire sky simultaneously in four infrared (IR) bands centred at 3.4, 4.6, 12, and $22\mu\text{m}$ (W1, W2, W3, and W4, respectively). We selected those stars that have measurements in W1 and W2 with a precision better than 0.05. We built the $(K_S - W1)$ against $(W1 - W2)$ and $(H - K_S)$ against $(W1 - W2)$ diagrams to classify the stars as either objects with disk or diskless, following the criteria described in Koenig et al. (2012) and Koenig & Leisawitz (2014). We cannot utilise diagrams based on the W3 or W4 bands, because dust emission from the molecular cloud dominates these bands for all sources in this area.

The results of this classification are represented in Fig. 16. Diskless stars are blue plusses, while stars with disks are green squares. We can observe that the majority of the

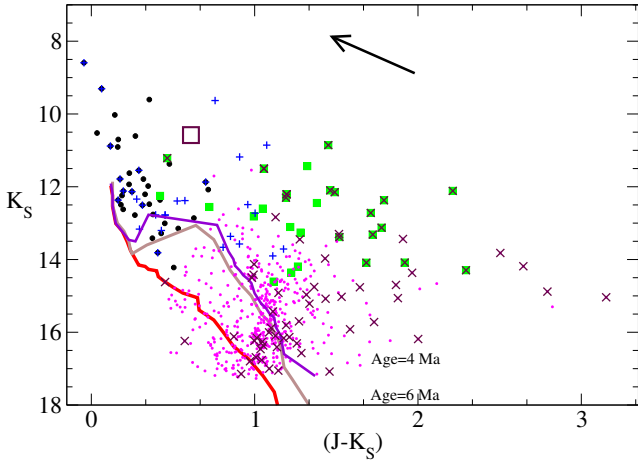


Figure 16. K_S magnitude against $(J-K_S)$ colour for Stock 8. See the text for a detailed explanation of the symbols. The arrow on the top is the standard reddening vector $A_{K_S} = 0.67 \cdot (J-K_S)$ of length $(J-K_S) = 0.5$ mag.

diskless stars are B-type likely members already on the main sequence or stars not considered members (field stars). All green squares are placed on the right side of the diagram. This is only natural, as they should have an excess in the $(J-K_S)$ colour arising from the disk. We have to emphasize that the limiting magnitude reached by WISE corresponds in most cases to stars with $K_S \approx 14$ in this area. Moreover, WISE images have much worse spatial resolution than our IR images. For these two reasons, most of the stars seen in our IR diagram have no WISE counterpart, either because they are too faint or because of confusion. The WISE objects with disks therefore must represent a population of moderately massive PMS stars ($M \geq 3M_\odot$).

To complement this analysis, we can use the $(J-H) - (H-K_S)$ diagram, or equivalently the IR Q reddening-free index. Stars with disks or strong infrared excess have negative values of Q (Negueruela et al. 2007). The use of this index to identify different types of red luminous stars is discussed by Messineo et al. (2012) and González-Fernández et al. (2015). Red giants have $Q \geq 0.35$. In Fig. 16, we plot with crosses stars having $Q < -0.1$. Most of the stars classified as PMS stars with disk from the WISE analysis are also selected by this criterion. In addition, this population extends to fainter magnitudes, covering the same range of $(J-K_S)$. We interpret them as lower mass PMS objects.

The degree of contamination by background stars is very low. There are very few stars with $Q > 0.35$ in our sample. Almost all of them are very faint, with $K_S \approx 16-17$ mag. They must therefore be field red dwarfs. In Fig. 16, we show with a large empty square the approximate position of unreddened red clump stars at the distance of the cluster, using typical photometric intrinsic parameters (Alves 2000; Cabrera-Lavers et al. 2005). If we project this locus along the reddening vector (indicated on the top of Fig. 16), we can see that very few stars are compatible with being background red giants. Indeed, most of the stars in this part of the diagram are PMS stars with disk according to the WISE criteria. This is not surprising, as we are looking at a distant cluster in the direction of the Anticenter. The background contamination must thus be low.

4 DISCUSSION

We have studied a region with a size of $\sim 40' \times 40'$ located close to the known open cluster Stock 8. Much of this area shows evidence for dust emission. We provide spectral types for almost all the cataloged early-type stars in the region, many of which are part of a diffuse population scattered over the field. Our spectral types confirm that all of them are early-type stars (see Tables 5 and 6). The spectral types range between O7.5V and B4III. The surface distribution of all the OB stars in the region can be seen in Fig 17. The population can be roughly divided in two clumps. The first one, to the north, comprising Alicante 11 and Alicante 12 and a few other stars, lies in the area devoid of dust emission (Fig. 1) and with weak $H\alpha$ emission (Fig. 17). The second one, on the southern half of the field, is formed by Stock 8 and a large population of stars scattered to the west of the cluster. This second group lies in an area showing evidence for diffuse dust emission and stronger $H\alpha$ emission. The spectral types observed, however, do not evidence any difference in age between the two groups, with the earliest spectral type found in the northern clump.

We have obtained a common distance of $2.80^{+0.27}_{-0.24}$ kpc ($DM = 12.2 \pm 0.2$) for the three open clusters in the area studied (Stock 8, Alicante 11 and Alicante 12) and an age between 4–6 Ma for Stock 8. These values are compatible with the previous estimation of the distance ($DM = 12.4$) for Stock 8 by Mayer & Macak (1971). They show rather worse agreement with the values of $DM = 11.4$ of Malysheva (1990) and $d = 2.05^{+0.1}_{-0.1}$ kpc ($DM = 11.6$) of Jose et al. (2008). The discrepancy with Malysheva (1990) is likely due to her derivation of an age of 12 Ma (at least double than the value that we find, 4–6 Ma). Her analysis, based on photographic photometry, cannot be so accurate as Strömgren photometry combined with spectroscopy. The presence of several O-type stars in the area and the PMS population in Stock 8 rule out such a high age. In the case of Jose et al. (2008), the discrepancy can have two procedural reasons. The main one is the value adopted for the reddening in calculating the distance. The reddening is variable because of the presence of the parental cloud, and for this reason, we have used individual values for B-type members. The second reason is our choice of the ZAMS as a lower envelope to the position of cluster stars. Conversely, their fit in their Fig. 9 is almost an upper envelope to the early-type stars (perhaps, again, because of their value for the reddening). Given the width of the main sequence, this difference alone can account for 0.3 or 0.4 mag in the DM derived.

4.1 Morphology of the region

The most remarkable feature in the region is the bright $H\alpha$ and dust shell lying immediately to the east of Stock 8 (Figures 1 and 9). This shell, which is also bright in radio (Jose et al. 2008), must be ionized by some of the OB stars in its vicinity. Jose et al. (2008) suggest that LSV +34°29, the brightest star in Stock 8, can emit enough ionizing photons to account for the photoionisation of the whole shell. In spite of this, they argue that the O-type stars LSV +34°18 and LSV +34°21 can contribute to the ionizing flux. However, we note that these two stars are much more reddened than any other OB star in the area (compare their V and K_S in

Table 5), and seem to be partially immersed in dust in the WISE image.

Our new spectral type for LSV +34°23 (HD 35633), O8 II(f), undoubtedly means that this is the main source of ionizing photons in the area. The morphology of the shell is perfectly compatible with this (see Figures 1 and 9). This star was classified as B0IV by Morgan et al. (1953). This classification is almost certainly due to a misidentification. Simón-Díaz & Herrero (2014) classify it as O7.5II(f)(n) in good agreement with our value. They measure a $v \sin i \approx 170 \text{ km s}^{-1}$. LSV +34°23 is the only star in the area that is clearly evolved away from the ZAMS². As such, it provides the only estimate of the age of the cluster from the massive stars. Comparison to typical spectral types in very young open clusters suggests an age of $\sim 4\text{--}5$ Ma. This value matches well the age obtained by using the PMS isochrones in Fig. 16.

A second feature of high interest is the apparent filamentary structure extending to the east of the H II shell that Jose et al. (2008) call the Nebulous Stream. This structure contains a stream of embedded sources and an obscured cluster known as CC 14 (see Figure 1). Even though Ivanov et al. (2005) studied the possibility that this is a massive and distant cluster, Jose et al. (2008) conclude that it is a small embedded cluster, associated to the stream of young objects. They also find that all these YSOs are younger than Stock 8. Indeed, the images suggest that the filament is not directly associated to Stock 8. The wide-field H α image (see Fig. 17) shows a bright filament of H II emission that is probably marking a photoionisation front that appears almost perpendicular to our line of sight in projection. The only star that can ionize this filament is LSV +34°36 (BD +34°1058). This star, situated to the north of Stock 8 and in relative isolation, is an SB2 with integrated spectral type O8 V that probably contains a moderately-luminous O-type star.

As discussed in Sect. 3.2.8, the hypothesis that all the OB stars that we have observed are at the same distance is perfectly consistent with observations. Unfortunately, there is no CCD optical photometry available in the literature for the area to the west of the cluster containing a large number of early-type stars to study if there is an underlying population of stars accompanying the concentration of 6 OB stars in an area $\sim 3' \times 4'$ (LSV +34°11, 13, 15, 16, 18 and 21), which could represent a diffuse cluster similar to Alicante 11. However, observation of 2MASS images and simple star counts in the 2MASS catalog suggest that, even though most of the OB stars are outside the area covered by our photometry, most of the intermediate-mass stars are inside the area covered. This configuration is very reminiscent of that found in the very young open cluster NGC 1893, which also sports a number of OB stars at some distance of the cluster core, in a region where there are essentially no intermediate-mass stars (Negueruela et al. 2007).

4.2 History of star formation in the region

Kang et al. (2012) have suggested the presence of a large-

scale star-formation structure in this area. They present the results of H I 21 cm-line observations to explore the nature of the high-velocity H I gas at $l \approx 173^\circ$. They designated this feature as Forbidden Velocity Wing (FVW) 172.8+1.5. Since this direction lies very close to the Galactic Anticentre, the Galactic rotation curve predicts very low radial velocities, and high-velocity components are not expected. FVW 172.8+1.5 seems to be associated with the H II complex G173+1.5, interpreted as one the largest star-forming regions in the outer Galaxy. Kang et al. (2012) consider that the complex is composed by two groups of Sharpless H II regions and a surrounding population of OB stars, distributed along a radio continuum loop of size $4.4^\circ \times 3.4^\circ$. The geometry of the area (in two dimensions) can be seen in their Fig. 5.

Two groups of H II regions can be seen in the area studied by Kang et al. (2012). To the northeast, the H II regions Sh 2-231, Sh 2-232, Sh 2-233 and Sh 2-235 have been claimed to be associated with a single molecular cloud. The distances determined by the spectrophotometry of the exciting stars of the individual H II regions are between 2.3 kpc and 1.0 kpc, while their radial velocities are: -18.1 ± 0.9 , -23 ± 0.5 , -18.4 ± 0.5 and -18.8 ± 1.7 , respectively (from the catalogue of Blitz et al. 1982). Kang et al. (2012) adopt a distance of 1.8 kpc, after Evans & Blair (1981). However, a recent comprehensive study of the extinction in this area (Straizys et al. 2010) finds a lower distance of 1.3 kpc for the complex (though these authors suggest that Sh 2-231 may not belong to the complex, but rather be a background object with a much higher distance). Since this distance is compatible with the estimate for Aur OB1 found by Humphreys (1978) from a few isolated OB stars, Straizys et al. (2010) identify the complex as the core of Aur OB1. To the southwest, the H II regions Sh 2-234 and Sh 2-237 are associated with the open clusters Stock 8 and NGC 1931, respectively.

Kang et al. (2012) assume that all the high-velocity structures in the area are connected, concluding that the H I-line feature FVW 172.8+1.5 is well correlated with a radio continuum loop, and the two seem to trace an expanding shell. The expansion velocity of the shell would be 55 km s^{-1} (well beyond the velocities allowed by Galactic rotation) and the kinetic energy of the shell would then be 2.5×10^{50} erg, suggesting that it represents an old (~ 0.33 Ma) supernova remnant produced inside this complex. They propose that the progenitor belonged to a stellar association near the center of the shell, and that this association could have triggered the formation of the OB stars currently exciting the H II regions on both edges of the shell. The H II complex G173+1.5 would then be an excellent example of sequential star formation over several stellar associations.

Our data do not seem to provide support for this interpretation. A close connection between Stock 8 and NGC 1931 seems unlikely, in spite of their proximity on the sky. The radial velocities of the associated molecular clouds are $-13.4 \pm 0.7 \text{ km s}^{-1}$ and $-4.3 \pm 0.7 \text{ km s}^{-1}$, respectively (as measured by CO velocities in Blitz et al. 1982). Fich et al. (1990) observed the radial velocity and line width of H α emission from 284 objects listed in Galactic H II regions catalogs. The values measured for Sh 2-234 and Sh 2-237 were $-14.3 \pm 0.5 \text{ km s}^{-1}$ and $+1.4 \pm 0.4 \text{ km s}^{-1}$, respectively. Differences of a few km s^{-1} are regularly observed between the cold and ionized components (Fich et al. 1990), as is the case

² As commented before, LSV +34°29 (BD +34°1054) has spectral type O9.7IV (see Table 5), but this is very likely a composite spectrum.

for Sh 2-237. However, the values of radial velocities from both measurements for Sh 2-234 (Stock 8) match within errors. This does not suggest the presence of perturbed gas, as would be expected if star formation was triggered by a shock wave. Moreover, the geometry of the shell, as discussed in the previous section, clearly demonstrates that it is ionized by stars to its west, and this is very difficult to reconcile with a shock wave coming from the east as the triggerer of star formation.

Independently of these measurements, the main difficulty with the scenario proposed by Kang et al. (2012) is the lack of cataloged OB stars inside the giant shell. If the supernova happened 0.33 Ma ago, it cannot have triggered the formation of a cluster that is $\gtrsim 4$ Ma old. Kang et al. (2012) suggest that the progenitor of the supernova was part of a population that might have triggered large-scale star formation, but there are very few stars that could belong to this population. The only O-type star that has a DM perhaps compatible is the multiple system LY Aur (Mayer 2013).

We have searched the catalog of Wouterloot & Brand (1989) for other molecular clouds that could be associated to Sh2-234. Wouterloot & Brand (1989) looked for CO(1-0) emission in the direction of 1302 IRAS sources with colours of star forming regions. The only measurement in the vicinity of Stock 8 is IRAS 05274+3345, which is located $\sim 27'$ to the southwest of NGC 1931 and $\sim 50'$ to the southeast of Stock 8. This compact H II region is associated with a small young embedded cluster, containing perhaps two massive stars (Chen 2005). Its radial velocity of $-3.90 \pm 0.20 \text{ km s}^{-1}$ is identical within errors to that of NGC 1931, and quite different from that of Sh2-234. Therefore, given the small separation in the sky, it seems that NGC 1931 and IRAS 05274+3345 are physically connected, but Stock 8 is not. The distance to NGC 1931 has recently been found to be 2.3 kpc by two different groups (Pandey et al. 2013; Lim et al. 2015). The difference in radial velocity and the morphology of WISE images is compatible with a slightly longer distance for Stock 8.

The age that we find for Stock 8 is relatively high for a cluster still associated with nebulosity. It is also remarkable that most of the O-type stars in the area are not directly associated with the nebulosity. In particular, Alicante 11, which contains at least two O-type stars, including the earliest spectral type in the region, is completely devoid of any nebulosity. These characteristics suggest that star formation has essentially stopped in this area. The H II region that we see represents the last remnant of a large cloud, illuminated by the O-type stars that formed from this cloud, and Stock 8 is emerging from the parental cloud as it photo-dissociates. This scenario is supported by the radio-continuum and CO images of the area presented by Kang et al. (2012), which show that the molecular cloud associated with Stock 8 is very small compared to the GMC associated with IC 410, or even that connected to Sh 2-232–235.

Remarkably, the embedded population seems to have the same age as the OB population – with the possible exception of objects in the Nebulous Stream. This is in contrast to the situation observed in W3, or in NGC 1893, where massive PMS stars (Herbig Be stars) are spatially segregated from main-sequence objects. Therefore the area surrounding Stock 8 does not seem to have fostered sequential star formation.

4.3 Position in the Milky Way

The current understanding of Galactic structure towards the Anticentre and in the third quadrant is very poor, in spite of many important recent developments. Several models of the structure and dynamics of the Galaxy have been published in the past few years, based on improved information (e.g. Bobylev & Bajkova 2010; McMillan & Binney 2010; Honma et al. 2012; Vallée 2015). In particular, Reid et al. (2014) have used more than 100 trigonometric parallaxes and proper motions for water and methanol masers associated with high-mass star-forming regions, measured by Very Long Baseline Array (VLBA), VLBI Exploration of Radio Astrometry (VERA) and the European VLBI Network (EVN), to fit axially symmetric models of the Milky Way. In their model (see their Fig. 1, and also Choi et al. 2014), the Perseus arm lacks tracers between $\sim 135^\circ$ and $\sim 170^\circ$. Choi et al. (2014) identify a single tracer close to Stock 8, the small embedded cluster IRAS 05168+3634 ($l = 170^\circ 7'$), with a parallax distance of 1.9 ± 0.2 kpc and a radial velocity of $v_{\text{LSR}} = -15.5 \pm 1.9 \text{ km s}^{-1}$ (Sakai et al. 2012). These values seem compatible with the Sh 2-231–235 complex, which is located $\sim 4^\circ$ away. Reid et al. (2014) also identify a number of tracers of the Perseus arm between $l = 184^\circ$ and 193° , all of them with distances $d \lesssim 2$ kpc, slightly shorter than their best fit for the arm, which gives a distance of ~ 2 kpc around $l \sim 180^\circ$. The typical width of the spiral arm should be around 0.5 kpc on each side of its mid-point.

With these characteristics, our distance to Stock 8 is just compatible with a location in the Perseus arm, within errors. We have to caution, however, that the simple picture of Galactic structure based on four main arms is not shared by many authors. The Orion arm, as observed by Xu et al. (2013) is a major structure. According to some authors, it extends for many kpc towards $l = 240^\circ - 250^\circ$, intersecting the Perseus and even the Outer arm (Vázquez et al. 2008; Costa 2015). On the other hand, the Perseus arm is very poorly traced beyond $l = 193^\circ$. All the possible tracers given by Reid et al. (2014) lie at very large distances from their fit. Conversely, a large number of stellar tracers seem to lie between the Orion and the Perseus arm all the way between $l = 180^\circ$ and $l = 240^\circ$, perhaps suggesting a more fluffy structure.

4.4 Is there an association Aur OB2?

As mentioned in the Introduction, in the classical list of OB associations by Humphreys (1978), Aur OB2 was described as composed by the open clusters Stock 8 and NGC 1893, together with some OB stars lying between them. However, all modern studies of NGC 1893 that make use of its upper main-sequence obtain distances ~ 5 kpc (Fitzsimmons 1993; Massey et al. 1995; Marco & Negueruela 2002; Negueruela et al. 2007). Other works using fits to the low-mass star sequence tend to give lower distances (around 3.5 kpc; Sharma et al. 2007; Prisinzano et al. 2011; Lim et al. 2014). The reasons for this discrepancy are unclear. Lim et al. (2014) attribute it to the inaccuracies in the spectroscopic parallaxes. However, given the almost universal (hidden) multiplicity of OB stars, spectroscopic parallaxes based on calibrations will most likely underestimate (rather than overestimate) the distance. Whatever the case, the distances to NGC 1893 and Stock 8 are not compatible, and the radial velocities

(v) We have detected a pre-main sequence population associated with the likely B-type members lying on the main sequence. From analysis of WISE and 2MASS data, we find that many of them present disks, also showing an excess in the ($J - K_S$) colour.

(vi) Star LSV +34°23 (HD 35633), located NW of Stock 8, has spectral type O8II(f), and is likely the main source of ionization in the nebula in the cluster region.

(vii) The picture that emerges is that of an area of recent star formation, where the H II region Sh 2-234 represents the last remnant of the cloud, and there is only some residual ongoing star formation, concentrated towards the Nebulous Stream and the small obscured cluster CC 14.

(viii) The classical picture of Aur OB2, as a concentration of OB stars extending between Stock 8 and NGC 1893 cannot be held, as NGC 1893 is clearly more distant. Stock 8 and the surrounding association are likely located on the Perseus arm, as defined by Choi et al. (2014). Other nearby H II regions, such as Sh 2-237 or the Sh 2-231 – 235 complex are also likely located on the Perseus arm, but their differing radial velocities and distances do not support a close connection with Stock 8 and the surrounding association.

ACKNOWLEDGEMENTS

We thank the referee for the careful reading of the manuscript.

This research is partially supported by the Spanish Ministerio de Ciencia e Innovación (MICINN) under grants AYA2012-39364-C02-02 and AYA2015-68012-C2-2-P, and by the Generalitat Valenciana (ACOMP/2014/129). AM acknowledges support from the Generalitat Valenciana through the grant BEST/2015/242 and from the Ministerio de Educación, Cultura y Deporte through the grant PRX15/00030.

This work is based in part on observations obtained with the Jacobus Kapteyn Telescope operated on the island of La Palma by the Isaac Newton Group, in the Spanish Observatorio Roque de los Muchachos of the Instituto de Astrofísica de Canarias.

This work is based in part on observations made with the Italian Telescopio Nazionale Galileo (TNG) operated on the island of La Palma by the Fundación Galileo Galilei of the INAF (Istituto Nazionale di Astrofisica) at the Spanish Observatorio del Roque de los Muchachos of the Instituto de Astrofísica de Canarias.

Based on observations made with the Nordic Optical Telescope, operated on the island of La Palma jointly by Denmark, Finland, Iceland, Norway, and Sweden, in the Spanish Observatorio del Roque de los Muchachos of the Instituto de Astrofísica de Canarias.

Some of the data presented here have been taken using ALFOSC, which is owned by the Instituto de Astrofísica de Andalucía (IAA) and operated at the Nordic Optical Telescope under agreement between IAA and the NBIfAFG of the Astronomical Observatory of Copenhagen.

Based in part on observations made at Observatoire de Haute Provence (CNRS), France.

This research has made use of the Simbad database, operated at CDS, Strasbourg (France) and of the WEBDA database, operated at the Institute for Astronomy of the

University of Vienna. This publication makes use of data products from the Two Micron All Sky Survey, which is a joint project of the University of Massachusetts and the Infrared Processing and Analysis Center/California Institute of Technology, funded by the National Aeronautics and Space Administration and the National Science Foundation.

REFERENCES

- Alves, D. R. 2000, *ApJ*, 539, 732
 Bik, A., Henning, Th., Stolte, A., et al. 2012, *ApJ*, 744, 87
 Blaauw, A. 1964, *ARA&A*, 2, 213
 Blitz, L., Fich, M., & Stark, A.A. 1982, *ApJS*, 49, 183
 Bobylev, V.V., & Bajkova, A.T. 2010, *MNRAS* 408, 1788
 Cabrera-Lavers, A., Garzón, F., & Hammersley, P. L. 2005, *A&A*, 433, 173
 Chen, Y., Yao, Y., Yang, J., Zeng, Q., & Sato, S. 2005, *ApJ*, 629, 288
 Choi, Y.K., Hachisuka, K., Reid, M.J., et al. 2014, *ApJ*, 790, 99
 Churchwell, E., Babler, B. L., Meade, M. R., et al. 2009, *PASP*, 121, 213
 Costa, E., Moitinho, A., Radiszcz, M., et al. 2015, *A&A*, 580, A4
 Crawford, D. L., & Mander, J. 1966, *AJ*, 71, 114
 Crawford, D. L., & Barnes, J. V. 1970a, *AJ*, 75, 978
 Crawford, D. L., Glaspey, J. W., & Perry, C. L. 1970b, *AJ*, 75, 822
 Crawford, D. L. 1975, *PASP*, 87, 481
 Draper, P.W., Taylor, M., & Allan, A. 2000, *Starlink User Note* 139.12, R.A.L.
 Drechsel, H., Haas, S., Lorenz, R., & Mayer, P. 1994, *A&A*, 284, 853
 Evans, N. J., II, & Blair, G. N. 1981, *ApJ*, 246, 394
 Fich, M., Treffers, R.R., & Dahl, G.P. 1990, *AJ*, 99, 622
 FitzGerald, M.P. 1970, *A&A*, 4, 234
 Fitzsimmons, A. 1993, *A&AS*, 99, 15
 Foster, T., & Brunt, C.M. 2015, *AJ*, 150, 147
 France, K., McCandliss, S.R., Burgh, E.B., & Feldman, P.D. 2004, *ApJ*, 616, 257
 Froebrich, D., Scholz, A., & Raftery, C. L. 2007, *MNRAS*, 374, 399
 Garmany, C. D., & Conti, P. S. 1984, *ApJ*, 284, 705
 Gillet, D., Burnage, R., Kohler, D., et al. 1994, *A&AS*, 108, 181
 González-Fernández, C., Dorda, R., Negueruela, I., & Marco, A. 2015, *A&A*, 578, A3
 Hardorp, J., Theile, I., & Voigt, H.H. 1965, *Hamburger Sternw., Warner & Swasey Obs.*, 5
 Hiltner, W. A. 1956, *ApJS*, 2, 389
 Hindson, L., Thompson, M. A., Urquhart, J.S., et al. 2013, *MNRAS*, 435, 2003
 Honma, M., Nagayama, T., Ando, K., et al. 2012, *PASJ*, 64, 136
 Howarth, I., Murray, J., Mills, D., & Berry, D.S. 1998, *Starlink User Note* 50.21, R.A.L.
 Humphreys, R. M. 1978, *ApJS*, 38, 309
 Ivanov, V. D., Borissova, J., Bresolin, F., & Pessev, P. 2005, *A&A*, 435, 107
 Jarrett, T. H., Cohen, M., Masci, F., et al. 2011, *ApJ*, 735, 112
 Johnson, H.L., & Morgan, W.W. 1953, *ApJ*, 117, 313
 Jose, J., Pandey, A.K., Ojha, D.K., et al. 2008, *MNRAS*, 384, 1675
 Kang, J.H., Koo, B.C., & Salter, C. 2012, *AJ*, 143, 75
 Kiminki, M.M., Kim, J.S., Bagley, M.B., Sherry, W.H., & Rieke, G.H. 2015, *ApJ*, 813, 42
 Koenig, X. P., Leisawitz, D.T., Benford, D.J., et al. 2012, *ApJ* 744, 130
 Koenig, X. P., Leisawitz, D. T. 2014, *ApJ*, 791, 131

- Kronberger, M., Teutsch, P., Alessi, B., et al. 2006, *A&A*, 447, 921 et al. 1971, *GCVS3*
- Lim, B., Sung, H., Kim, J.S., Bessel, M.S., & Park, B.-G. 2014, *MNRAS*, 443, 454
- Lim, B., Sung, H., Bessel, M.S., et al. 2015, *AJ*, 149, 127
- McMillan, P.J., & Binney, J.J. 2010, *MNRAS*, 402, 934
- Malysheva, L. K. 1990, *Soviet Astronomy*, 34, 122
- Manfroid, J. 1993, *A&A*, 271, 714
- Marco A., Bernabeu, G., & Negueruela I. 2001, *AJ*, 121, 2075
- Marco A., & Negueruela I. 2002, *A&A*, 393, 195
- Marco A., & Negueruela I. 2013, *A&A*, 552, 92
- Massey, P., Johnson, K.E., & DeGioia-Eastwood, K. 1995, *ApJ*, 454, 151
- Mayer, P. 1964, *Acta Univ. Carol. Math. Phys.*, 1, 25M
- Mayer, P., & Macak, P. 1971, *Bull. Astron. Inst. Czech.*, 22, 46
- Mayer, P., Drechsel, H., Harmanec, P., Yang, S., & Slechta, M. 2013, *A&A*, 559, A22
- Messineo, M., Menten, K. M., Churchwell, E., & Habing, H. 2012, *A&A*, 537, A10
- Messineo, M., Clark, J.S., Figer, et al. 2015, *ApJ*, 805, 110
- Morgan, W.W., Whitford, A.E., & Code, A.D. 1953, *ApJ*, 118, 318
- Morgan, W.W., Code, A.D., & Whitford, A.E. 1955, *ApJS*, 2, 41
- Negueruela I., & Marco A. 2003, *A&A*, 406, 119
- Negueruela I., Marco A., Israel, G.L., & Bernabeu G. 2007, *A&A*, 471, 485
- Netopil, M., Paunzen, E., & St̃ijtz, Christian., 2012, *ASSP*, 29, 53
- Pandey, A.K., Sharma, S., Upadhyay, K., et al. 2007, *PASJ*, 59, 547
- Pandey, A.K., Eswaraiah, C., Sharma, S., et al. 2013, *ApJ*, 764, 172
- Perry, C. L., Lee, P. D., & Barnes, J. V. 1978, *PASP*, 90, 73
- Perry, C. L., Olsen, E. H., & Crawford, D. L. 1987, *PASP*, 99, 1184
- Preibisch, T., & Zinnecker, H. 2007, *Triggered Star Formation in a Turbulent ISM*, Edited by B. G. Elmegreen and J. Palous. *Proceedings of the International Astronomical Union 2, IAU Symposium 237*, held 14-18 August, 2006 in Prague, Czech Republic. Cambridge: Cambridge University Press, 2007., pp.270-277
- Preibisch, T., Ratzka, T., Kuderna, B., et al. 2011, *A&A*, 530, 34
- Prisinzano, L., Sanz-Forcada, J., Micela, G., et al. 2011, *A&A*, 527, A77
- Reid, M.J., Menten, K.M., Brunthaler, A., et al. 2014, *ApJ*, 783, 130
- Román-Zúñiga, C.G., Ybarra, J.E., Megías, G.D., et al. 2015, *AJ*, 150, 80
- Sakai, N., Honma, M., Nakanishi, H., et al. 2012, *PASJ*, 64, 108
- Sharma, S., Pandey, A.K., Ojha, D.K., et al. 2007, *MNRAS*, 380, 1141
- Shortridge, K., Meyerdicks, H., Currie, M., et al. 1997, *Starlink User Note 86.15*, R.A.L.
- Siess L., Dufour E., & Forestini M. 2000, *A&A*, 358, 593
- Simón-Díaz, S. & Herrero, A. 2014, *A&A*, 562, 135
- Skrutskie, M.F., Cutri, R.M., Stiening, R., et al. 2006, *AJ*, 131, 1163
- Sota, A., Maíz Apellániz, J., Walborn, N.R., et al. 2011, *ApJS*, 193, 24
- Sota, A., Maíz Apellániz, J., Morrell, N.I., et al. 2014, *ApJS*, 211, 10
- Stetson, P. B. 1987, *PASP*, 99, 191
- Straižys, V., Drew, J. E., & Laugalys, V. 2010, *Baltic Astronomy*, 19, 169
- Subramaniam A., & Sagar R. 1999, *AJ*, 117, 937
- Turner, D. 1980, *ApJ*, 240, 137
- Vallée, J.P. 2015, *MNRAS*, 450, 4277
- Walborn, N.R. 1971, *ApJS*, 23, 257
- Walborn, N. R., & Fitzpatrick, E. L. 1990, *PASP*, 102, 379
- Vázquez, R., May, J., Carraro, G., et al. 2008, *ApJ*, 672, 930
- Wouterloot, J.G.A., & Brand, J. 1989, *A&AS*, 80, 149
- Wright, E.L., Eisenhardt, P.R.M., & Mainzer, A.K. et al. 2010, *AJ*, 140, 1868
- Wright, N.J., Parker, R.J., Goodwin, S.P., & Drake, J.J. 2014, *MNRAS*, 438, 639
- Xu, Y., Li, J. J., Reid, M. J. et al. 2013, *ApJ*, 769, 15

6 PHOTOMETRIC TABLES

This paper has been typeset from a \TeX/L\AA\TeX file prepared by the author.

Table 10. Coordinates in J2000 for stars with optical photometry in the cluster Stock 8. The second column indicates its number in Table 11, where we present our TNG photometry. The 2MASS photometry values are given for stars with no measurement in Table 11. Material on-line

Name	Number	RA(J2000)	DEC(J2000)	J	σ_J	H	σ_H	K_S	σ_{K_S}
ST1		05:27:51.82	+34:30:48.1	9.075	0.027	8.441	0.020	8.219	0.018
ST2		05:28:06.39	+34:30:40.3	13.820	0.024	13.501	0.027	13.419	0.036
ST3		05:27:49.91	+34:30:43.7	12.767	0.019	12.592	0.019	12.492	0.023
ST4		05:28:15.51	+34:30:36.3	14.248	0.026	13.876	0.036	13.777	0.041
ST5		05:28:04.60	+34:30:36.6	14.359	0.023	13.979	0.031	13.743	0.040
ST6		05:28:09.92	+34:30:32.5	13.820	0.023	13.210	0.025	13.057	0.029

Table 11. Near-IR photometry obtained by us for stars in the cluster Stock 8. Material on-line

Name	R.A(J2000)	DEC(J2000)	J	σ_J	H	σ_H	K_S	σ_{K_S}
1	05:28:00.83	+34:22:44.7	17.168	0.013	16.393	0.016	15.986	0.013
2	05:28:15.89	+34:22:47.2	15.499	0.012	14.513	0.010	14.261	0.010
3	05:28:03.07	+34:22:45.5	14.585	0.010	14.168	0.009	14.049	0.009
4	05:28:13.87	+34:22:49.9	14.910	0.011	14.118	0.009	13.893	0.010
5	05:28:13.76	+34:22:50.4	15.220	0.013	14.380	0.011	14.131	0.011

Table 12. Optical photometry for stars in the open cluster Stock 8. The values with label * are not considered in the analysis because their photometric errors are around 0.1. Material on-line

Name	V	σ_V	$(b-y)$	$\sigma_{(b-y)}$	c_1	σ_{c_1}	N	m_1	σ_{m_1}	N	β	σ_β	N
ST1	11.435	0.021	0.964	0.027	-0.250	0.040	1	0.574	0.039	1	2.597	0.032	1
ST2	15.131	0.004	0.525	0.010	-0.135	0.036	3	0.252	0.060	3	2.616	0.052	2
ST3	13.568	0.034	0.353	0.008	0.367	0.037	6	0.347	0.025	5	2.803	0.029	5
ST4	15.859	0.008	0.629	0.038	0.124	0.111*	2	0.134	0.097*	2	2.603	0.040	2
ST5	15.947	0.045	0.678	0.009	-0.046	0.119*	2	0.179	0.075	2	2.597	0.061	2
ST6	15.864	0.002	0.762	0.013	0.031	0.200*	2	0.227	0.078	2	2.578	0.064	2

Table 13. Coordinates in J2000 and 2MASS photometry for stars with optical photometry in the new cluster Alicante 11. Material on-line

Name	RA(J2000)	DEC(J2000)	J	σ_J	H	σ_H	K_S	σ_{K_S}
Alicante 11-1	05:27:55.48	+34:50:21.3	10.858	0.018	10.234	0.016	10.062	0.017
Alicante 11-2	05:27:57.72	+34:49:25.5	12.051	0.019	11.788	0.018	11.683	0.020
Alicante 11-3	05:27:24.26	+34:49:26.0	11.243	0.022	11.113	0.027	11.003	0.019
Alicante 11-4	05:27:27.63	+34:48:53.7	12.208	0.023	11.886	0.030	11.812	0.023
Alicante 11-5	05:27:54.47	+34:48:43.7	12.982	0.021	12.815	0.022	12.749	0.023

Table 14. Optical photometry for stars in the new open cluster Alicante 11. The values with label * are not considered in the analysis because of their error are around 0.1. Material on-line

Name	V	σ_V	$(b-y)$	$\sigma_{(b-y)}$	m_1	σ_{m_1}	c_1	σ_{c_1}	β	σ_β	N
Alicante 11-1	13.225	0.029	0.863	0.047	0.308	0.071	0.292	0.066	2.689	0.045	1
Alicante 11-2	13.334	0.028	0.425	0.019	0.042	0.030	0.899	0.030	2.840	0.023	3
Alicante 11-3	12.201	0.007	0.313	0.017	0.074	0.026	0.476	0.018	2.790	0.022	5
Alicante 11-4	13.636	0.012	0.470	0.005	0.115	0.016	0.444	0.025	2.712	0.007	5
Alicante 11-5	13.860	0.023	0.327	0.035	-0.007	0.050	0.909	0.055	2.821	0.049	3

Table 15. Coordinates in J2000 and 2MASS photometry for stars with optical photometry in the new cluster Alicante 12. Material on-line

Name	RA(J2000)	DEC(J2000)	J	σ_J	H	σ_H	K_S	σ_{K_S}
Alicante 12-1	05:28:17.33	+34:51:57.0	13.027	0.021	12.689	0.019	12.590	0.025
Alicante 12-2	05:28:15.50	+34:51:51.4	12.557	0.019	12.198	0.018	12.098	0.023
Alicante 12-3	05:28:05.04	+34:51:41.2	11.829	0.019	11.672	0.019	11.562	0.022
Alicante 12-4	05:28:13.83	+34:51:24.1	11.504	0.019	11.173	0.018	11.108	0.019
Alicante 12-5	05:28:28.12	+34:50:34.6	11.743	0.018	11.551	0.016	11.466	0.019

Table 16. Optical photometry for stars in the open cluster Alicante 12. The values with label * are not considered in the analysis because of their error are around 0.1. Material on-line

Name	V	σ_V	$(b-y)$	$\sigma_{(b-y)}$	m_1	σ_{m_1}	c_1	σ_{c_1}	β	σ_β	N
Alicante 12-1	14.580	0.048	0.586	0.050	0.051	0.093*	0.423	0.040	2.732	0.097*	3
Alicante 12-2	14.250	0.019	0.607	0.011	0.026	0.041	0.511	0.008	2.740	0.046	2
Alicante 12-3	12.730	0.043	0.357	0.034	0.010	0.010	0.221	0.037	2.743	0.073	3
Alicante 12-4	12.855	0.036	0.486	0.032	0.106	0.066	0.520	0.047	2.716	0.057	3
Alicante 12-5	12.868	0.027	0.367	0.037	0.079	0.055	0.920	0.016	2.835	0.038	3